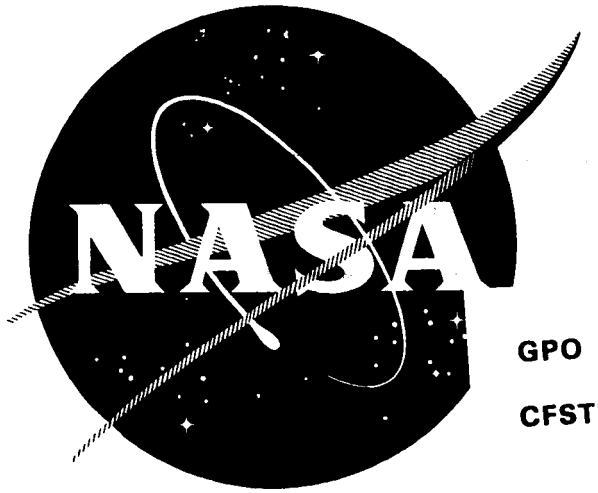
WANL-PR-(P)-011
NASA-CR-72073



GPO PRICE $ _____

CFSTI PRICE(S) $ _____

Hard copy (HC) $3.00

Microfiche (MF) .65

ff 653 July 65

DETERMINATION OF THE WELDABILITY AND ELEVATED TEMPERATURE STABILITY OF REFRACTORY METAL ALLOYS

Eleventh Quarterly Report

by

G. G. Lessmann and D. R. Stoner

prepared for
National Aeronautics and Space Administration
Lewis Research Center
Space Power Systems Division
Under Contract NAS 3-2540



ASTRONUCLEAR LABORATORY
WESTINGHOUSE ELECTRIC CORPORATION

N67-18695 (ACCESSION NUMBER) (THRU) (PAGES) (CODE) (NASA CR OR TMX OR AD NUMBER) (CATEGORY)
FACILITY FORM 602

NOTICE

This report was prepared as an account of Government-sponsored work. Neither the United States nor the National Aeronautics and Space Administration (NASA), nor any person acting on behalf of NASA:

A) Makes any warranty or representation, expressed or implied, with respect to the accuracy, completeness, or usefulness of the information contained in this report, or that the use of any information, apparatus, method, or process disclosed in this report may not infringe privately-owned rights; or

B) Assumes any liabilities with respect to the use of, or for damages resulting from the use of any information, apparatus, method or process disclosed in this report.

As used above, "person acting on behalf of NASA" includes any employee or contractor of NASA, or employee of such contractor, to the extent that such employee or contractor of NASA or employee of such contractor prepares, disseminates, or provides access to, any information pursuant to his employment or contract with NASA, or his employment with such contractor.

Copies of this report can be obtained from:

National Aeronautics & Space Administration
Office of Scientific and Technical Information
Washington 25, D. C.
Attention: AFSS-A

Astronuclear Laboratory

WANL-PR-(P)-011
NASA-CR-72073

DETERMINATION OF THE WELDABILITY AND ELEVATED TEMPERATURE STABILITY OF REFRACTORY METAL ALLOYS

by

G. G. Lessmann
and
D. R. Stoner

Eleventh Quarterly Report

Covering the Period

December 21, 1965 to March 20, 1966

Prepared for

NATIONAL AERONAUTICS AND SPACE ADMINISTRATION
Contract NAS 3-2540

Technical Management
NASA-Lewis Research Center
Cleveland, Ohio
Space Power Systems Division
Paul E. Moorhead

Astronuclear Laboratory
Westinghouse Electric Corporation
Pittsburgh 36, Pa.

ABSTRACT

The weldability of three tungsten alloys including W-25Re unalloyed W, and Sylvania "A" (W-O.5Hf-0.02C) was determined. All were evaluated as 0.035-inch sheet. Both W and W-25Re were converted from arc cast ingot whereas Sylvania "A" is a powder metallurgy product. Only nominal weldability was realized in these systems even with preheating to 550°F. All had poor weld ductility as demonstrated by high ductile-to-brittle transition temperatures. Only a minimal recovery of ductility was realized by post-weld annealing.

The effect of oxygen contamination on weld strength was determined at room and three elevated temperatures for T-111, T-222, and FS-85. The relationships of fracture mode and location, strength, and ductility with respect to thermal history over a wide oxygen contaminating range (to 1000 ppm) were determined and compared. All alloys are sensitive to contamination and, yet, demonstrated an impressive tolerance.

TABLE OF CONTENTS

		Page No.
	ABSTRACT	iii
I	INTRODUCTION	1
II	SUMMARY	3
III	TECHNICAL PROGRAM	4
	A. The Weldability of Tungsten and Tungsten Alloys	4
	B. Effect of Oxygen Contamination on Weldability	28
IV	FUTURE WORK	42
V	REFERENCES	65

LIST OF FIGURES

Figure No.	Title	Page No.
1	Summary of Bend Test Results Showing the Spread in Bend Ductile-to-Brittle Transition Temperatures Obtained Over a Practical Range of Welding Parameters.	5
2	Sheet Butt Weld Fixture with Heated Backup Bar for Welding Tungsten Alloys	7
3	Bead-on-Plate Patch Test of Unalloyed Tungsten	10
4	Typical TIG Butt Welds in Unalloyed Tungsten and W-25Re Sheet	11
5	Unalloyed Tungsten Sheet, Base Metal and TIG Weld Bend Test Results (4t Bend Radius)	12
6	TIG Weld Structure in Unalloyed Tungsten, Weld No. 1, Table 2 (Welded at 7.5 ipm Without Preheat)	13
7	Hardness Traverses of TIG Welds in Unalloyed Tungsten	14
8	Typical Sections of Electron Beam Welds in Unalloyed Tungsten	17
9	Typical Dye-Penetrant Results of Electron Beam Welds in Arc Cast Unalloyed Tungsten Sheet	18
10	Unalloyed Tungsten Sheet, EB Weld Bend Test Results (4t Bend Radius)	19
11	W-25Re Sheet, TIG Weld Bend Test Results (4t Bend Radius)	21
12	W-25Re Sheet, TIG Weld Bend Test Results (4t Bend Radius)	22
13	The Effect of Weld Parameters on Ductility of Gas Tungsten Arc Welds in W-25Re Alloy Sheet	23
14	Hardness Traverses of TIG Welds in W-25Re Sheet	25
15	Photomicrographs of Cast Weld Area in Gas Tungsten Arc Welded W-25Re Sheet	26
16	Photomicrographs of Cast Weld Area in Gas Tungsten Arc Welded W-25Re Sheet	27

LIST OF FIGURES (Continued)

Figure No.	Title	Page No.
17	Bead-on-Plate Patch Test of Sylvania "A"	29
18	Gas Tungsten Arc Butt Welds in Sylvania "A"	30
19	Program Outline for Contaminated Alloy Weldability Evaluation	33
20	T-111, Yield Strength Versus Temperature at 5 Oxygen Levels	44
21	T-111, Tensile Strength Versus Temperature at 5 Oxygen Levels	45
22	T-111, Elongation Versus Temperature at 5 Oxygen Levels	46
23	T-222, Yield Strength Versus Temperature at 5 Oxygen Levels	47
24	T-222, Tensile Strength Versus Temperature at 5 Oxygen Levels	48
25	T-222, Elongation Versus Temperature at 5 Oxygen Levels	49
26	FS-85, Yield Strength Versus Temperature at 5 Oxygen Levels	50
27	FS-85, Tensile Strength Versus Temperature at 5 Oxygen Levels	51
28	FS-85, Elongation Versus Temperature at 5 Oxygen Levels	52
29	T-111, Photographs of 1500°F Tensile Specimens	53
30	T-111, Photographs of 1800°F Tensile Specimens	54
31	T-111, Photographs of Room Temperature Tensile Specimens	55
32	T-111, Photographs of 2200°F Tensile Specimens	56
33	T-222, Photographs of 1500°F Tensile Specimens	57
34	T-222, Photographs of 1800°F Tensile Specimens	58
35	T-222, Photographs of Room Temperature Tensile Specimens	59

LIST OF FIGURES (Continued)

Figure No.	Title	Page No.
36	T-222, Photographs of 2200°F Tensile Specimens	60
37	FS-85, Photographs of 1500°F Tensile Specimens	61
38	FS-85, Photographs of 1800°F Tensile Specimens	62
39	FS-85, Photographs of Room Temperature Tensile Specimens	63
40	FS-85, Photographs of 2200°F Tensile Specimens	64

LIST OF TABLES

1.	Alloys Included in the Weldability and Thermal Stability Evaluation	2
2.	Unalloyed Arc Cast Tungsten Sheet, TIG Weld Record	9
3.	Unalloyed Arc Cast Tungsten Sheet, E. B. Weld Record	15
4.	W-25Re Sheet, TIG Weld Record	20
5.	Sylvania "A" Sheet, TIG Weld Record	31
6.	T-111, Tensile Properties Versus Temperature at 5 Oxygen Levels.	36
7.	T-222, Tensile Properties Versus Temperature at 5 Oxygen Levels	37
8.	FS-85, Tensile Properties Versus Temperature at 5 Oxygen Levels	38

I. INTRODUCTION

This is the Eleventh Quarterly Progress Report describing work accomplished under Contract NAS 3-2540. The objective of this program is to determine the weldability and long time elevated temperature stability of promising refractory metal alloys in order to select those most suitable for use in advanced alkali-metal space electric power systems. Alloys included in this investigation are listed in Table 1. A detailed discussion of the program and program objectives was presented in the First Quarterly Report.[1] As an addition to this program, an evaluation of the effect of oxygen contamination on the weldability and thermal stability of refractory metal alloys has been undertaken. Three alloys, including T-111, T-222, and FS-85 will be evaluated. A detailed discussion and outline of this study was presented in the Seventh Quarterly Report.[2]

Process and test controls employed throughout this program emphasize the important influence of interstitial elements on the properties of refractory metal alloys. Stringent process and test procedures are required, including continuous monitoring of the TIG weld chamber atmosphere, electron beam welding in a 10^{-6} torr vacuum, aging in furnaces employing hydrocarbon free pumping systems providing pressures less than 10^{-8} torr, and chemical sampling following successive stages of the evaluation for verification of these process controls.

Equipment requirements and set-up, and procedures for welding and testing, have been described in previous progress reports. Any improvements in processes, changes in procedures, or additional processes and procedures are described in this report.

TABLE 1 - Alloys Included in the Weldability and Thermal Stability Evaluations

Alloy	Nominal Composition Weight Percent
AS-55	Cb-5W-1Zr-0.2Y-0.06C
B-66	Cb-5Mo-5V-1Zr
C-129Y	Cb-10W-10Hf+Y
Cb-752	Cb-10W-2.5Zr
D-43	Cb-10W-1Zr-0.1C
FS-85	Cb-27Ta-10W-1Zr
SCb-291	Cb-10W-10Ta
D43 + Y	Cb-10W-1Zr-0.1C+Y
T-111	Ta-8W-2Hf
T-222	Ta-9.6W-2.4Hf-0.01C
Ta-10W	Ta-10W
W-25 Re	W-25Re
W	Unalloyed
Sylvania "A"*	W-0.5Hf-0.02C

* NOTE: All alloys from arc-cast and/or electron beam melted material except Sylvania "A"

II. SUMMARY

The weldability study of the tungsten alloys was completed. This terminated the first phase of this program in which the weldability of refractory metal alloys was determined. The tungsten alloys had poor weldability and were difficult to handle because of their low ductility at ambient temperatures. Weld cleavage failures occurred frequently during weld cooling through the ductile-brittle transition range to room temperature. In this respect, variability in weld ductility for different welding conditions seemed to result from differences in the magnitude and distribution of residual weld stress levels. Hence, twinning which is strain induced, was associated with the lowest ductility welds in W-25Re. Arc welding of W and W-25Re is weld speed limited to 15 ipm or less. Above this speed severe weld cleavage cracking occurs, probably reflecting a more severe residual stress distribution associated with higher welding speeds.

The size of weld and recrystallized area in tungsten alloys as determined by both unit length heat input and welding speed also influenced weld ductility. Smaller, lower heat input welds, had better ductility. Electron beam results (lowest heat input) confirm this trend as observed for gas tungsten arc welds. Preheat appeared to improve ductility in W-25Re arc welds, while results with unalloyed tungsten were inconclusive. A 1400°C post-weld stress relief was generally ineffective in improving ductility of arc welds in either W or W-25Re. W-25Re displayed an apparent tendency toward hot tearing as well as cleavage during welding.

Tensile behavior of welds in oxygen contaminated T-111, T-222 and FS-85 was determined for oxygen contamination levels (in the base metal prior to welding) between 70 and 1000 ppm. Test temperatures included ambient, 1500, 1800 and 2200°F. The basic observed relations of strength and ductility to contamination level were reasonably straightforward. Increasing oxygen increased strength and decreased ductility at all temperatures. Data interpretation as a means of screening these alloys based on "oxygen sensitivity" led to complex considerations of fracture behavior and strengthening mechanisms. All three alloys behaved in basically the same manner—no degradation of strength was observed even though differences in fracture behavior were noted.

III. TECHNICAL PROGRAM

A. WELDABILITY STUDY OF TUNGSTEN AND TUNGSTEN BASE ALLOYS

During this period the weldability study of the tungsten alloys was completed marking the termination of the weldability phase of this program. The gas-tungsten-arc weld results of unalloyed W, W-25Re, and Sylvania "A" are discussed below along with electron beam weld results for unalloyed W. Electron beam welding of W-25Re was previously reported[3] while the electron beam investigation of Sylvania "A" was eliminated because of extremely poor weldability displayed during the tungsten-arc weld study.

The tungsten alloys are categorized among the refractory metal alloys by their inferior ductility. This is shown graphically by the bend test summary of the alloys welded in this program, Figure 1. This figure shows the range of bend transition temperatures obtained for each alloy throughout a practical range of welding conditions. Despite the handicap of poor ductility, tungsten may be employed in special high temperature applications. Hence, these alloys were included in this program.

Tungsten retains a certain degree of ductility and fabricability in the wrought and stress relieved conditions. Hence, the stress-relieved structure was selected for this study as opposed to the recrystallized condition obtained in the tantalum and columbium alloys. Also, in tungsten alloys, the strengthening effect of a cold worked structure can be appreciated at temperatures exceeding 2000°F making this structure attractive in many potential applications. The W and W-25Re sheet was converted from arc cast ingots. The selection of arc cast material was based on a pre-procurement evaluation which demonstrated a pronounced decrease in weld porosity of arc cast sheet compared with conventional powder metallurgy sheet from several sources[2]. The Sylvania "A" sheet is the only powder metallurgy product evaluated in this program. Unlike the tantalum and columbium alloys, tungsten alloys were evaluated in 0.035-inch sheet only and not in plate thickness.

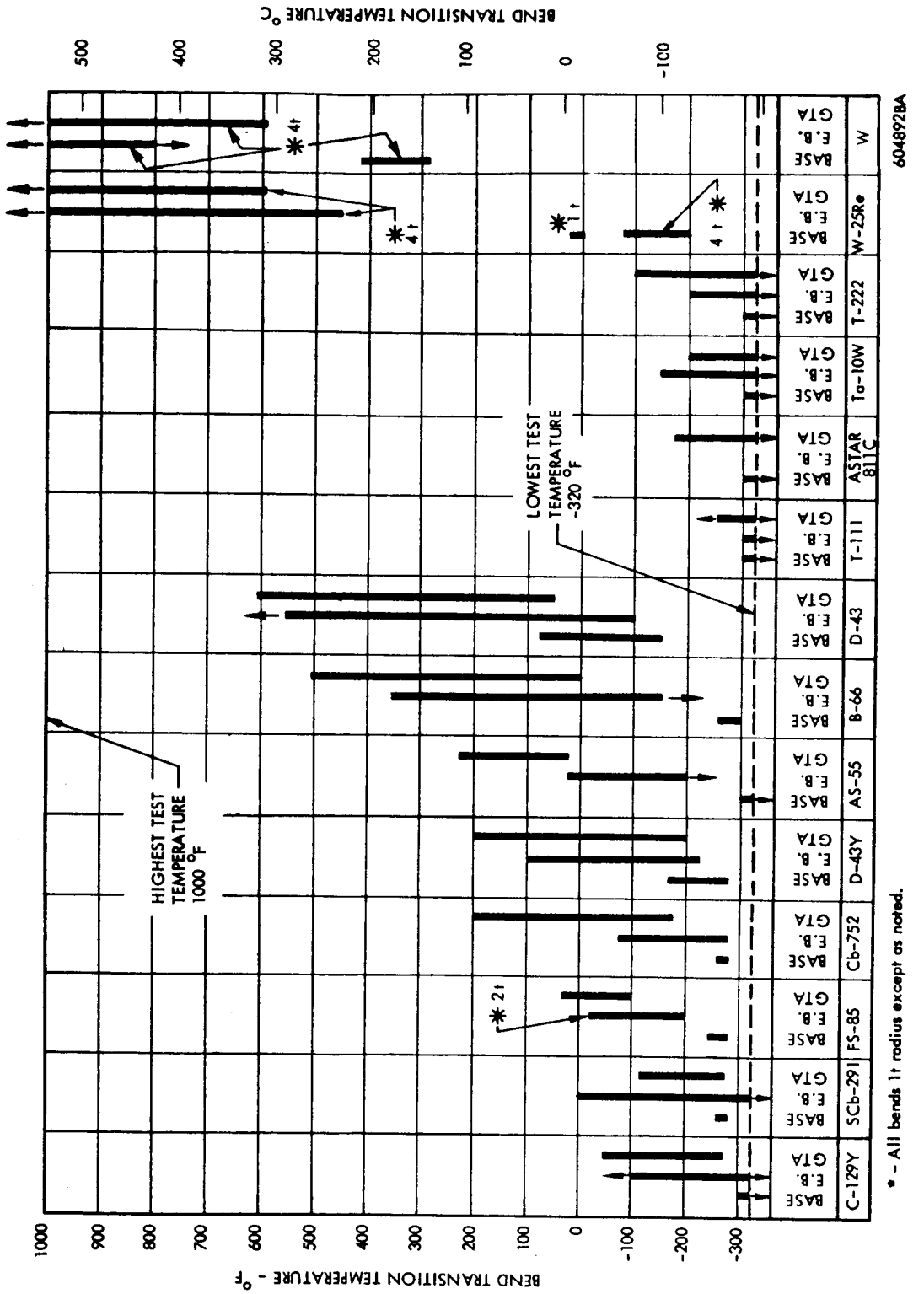


FIGURE 1 - Summary of Bend Test Results Showing the Spread in Bend Ductile-to-Brittle Transition Temperatures Obtained Over a Practical Range of Welding Parameters (Data for ASTAR 811C, Ta-8W-1Re1Hf-0.025C, Generated under Contract NAS 3-2592, Ref. 13)

The same general welding techniques and welding approach was employed in welding the tungsten alloys as used with the other alloys.[4,5] However, the effect of preheat in TIG welding was selected as an additional parameter in evaluating the tungsten alloys. Preheating was accomplished with heaters placed in the backup bar of the welding fixture. This provided a preheat of 550°F. The holding fixture is shown in Figure 2. The choice of other welding parameters to be evaluated was made in such a way that the unit weld length heat input, freezing and cooling rates, and weld size effects were emphasized as opposed to merely varying voltage, amperage, and speed per se. This varies in a qualitatively predictable manner the time-temperature relationships which control metallurgical structure, and, hence, mechanical properties. This approach proved particularly beneficial for the columbium alloys in providing an appreciation of responses to welding parameters and process effects.[6] Tungsten sheet was evaluated using 13 electron beam welding conditions and 10 gas tungsten arc parameter combinations. For the W-25Re sheet 18 electron beam and 12 gas tungsten arc weld combinations were employed. All attempts to weld Sylvania "A" proved unsuccessful.

Sample preparation for both welding and, after welding, for testing was considerably more complicated than for columbium and tantalum alloys. Specimen blanking by shearing was unsatisfactory because of edge cracking and possible delamination. Warm shearing at +600°F reduced this problem but did not eliminate it. Consequently, weld specimen blanking was accomplished by electro-discharge machining (EDM) and test specimen blanking was accomplished using an abrasive cut-off wheel. Edge finishing for butt weld specimens was accomplished by stacking and wet edge grinding prior to pickling and welding. The unalloyed tungsten and Sylvania "A", and the TIG welded W-25Re weld blanks were vacuum degassed for 1 hour at 2000°F after pickling and just before welding. This additional precaution in cleaning was based on our previous results in the columbium and tantalum alloy systems[6,7] in which adsorbed (physical and/or chemical) hydrogen and/or pickling residues, which were removable by degassing, appeared to be the source of weld porosity. The pickling solution employed for tungsten and tungsten alloys consisted of 9 parts hydrofluoric acid and 1 part concentrated nitric acid.

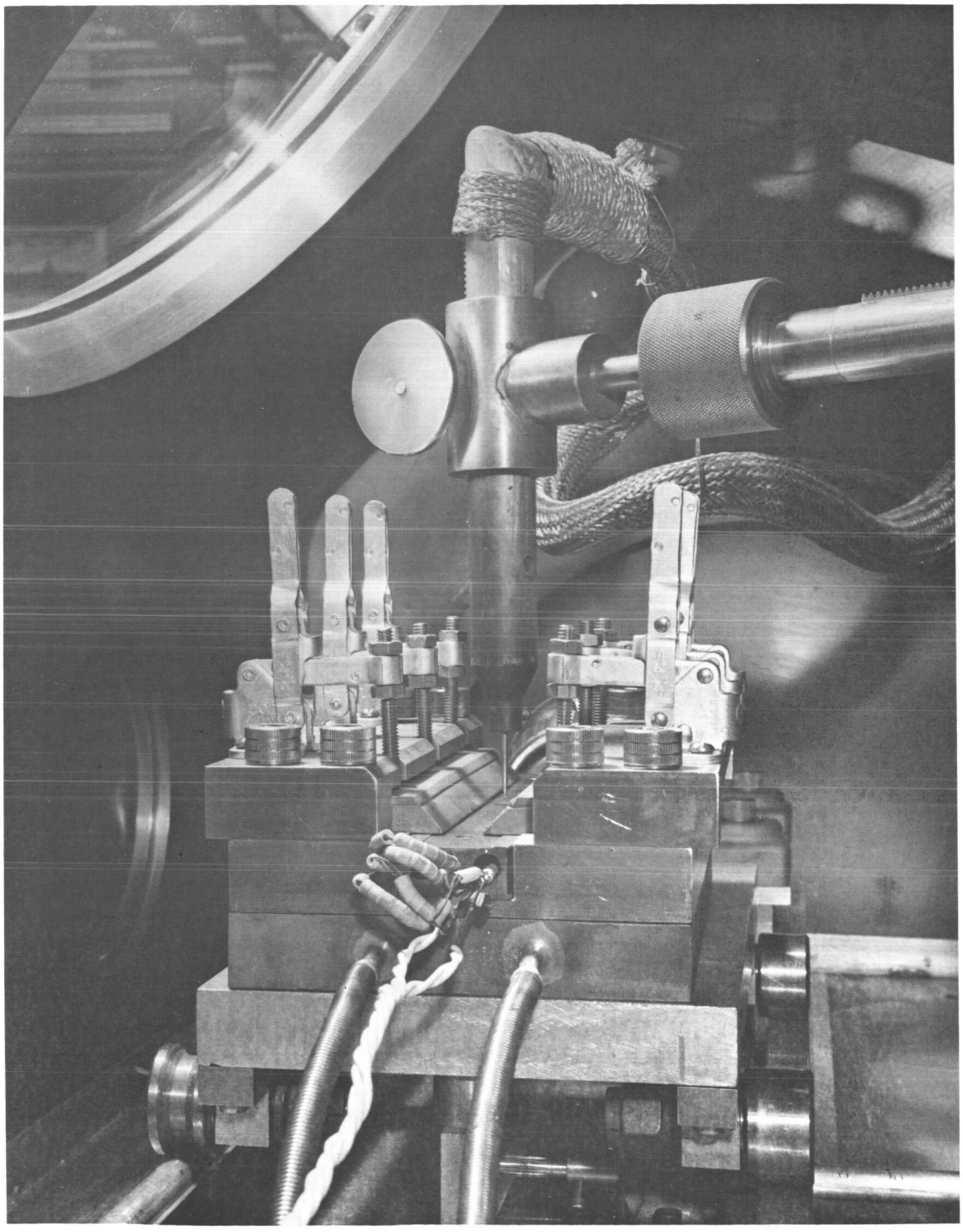


FIGURE 2 - Sheet Butt Weld Fixture with Heated Backup Bar for Welding Tungsten Alloys

Results: A discussion of the results of the weldability study is presented below for each tungsten alloy.

Unalloyed Tungsten, Gas Tungsten Arc Welding

Weld parameters employed in evaluating the weldability of unalloyed W are listed in Table 2 along with weld inspection results. Out of 10 parameter combinations, 6 welded successfully. The other 4 contained cleavage cracks. Four out of 6 good welds were obtained using a 550°F preheat indicating that this may be beneficial. Weldability decreased with increased welding speed such that satisfactory welds were obtained at 15 ipm but not at 30 ipm. For comparison, the columbium and tantalum alloys generally were weldable to 60 ipm or faster. The manual patch test produced in tungsten proved to be defect-free even though welded without preheat, Figure 3. Typical butt welds are shown in Figure 4.

The 4t bend transition temperature for the tungsten welds varied from +700°F to greater than +1000°F, Figure 5. This compares with a base metal transition temperature of about 400°F. A typical gas tungsten arc weld microstructure is shown in Figure 6. The large full section grains of the weld are largely responsible for the poor ductility of welds as compared with stress relieved base metal. The weld hardness traverses, shown in Figure 7, indicate a weld hardness of about 375 DPH and base metal hardness (stress relieved) of about 475 DPH. A peak hardness of near 500 DPH at the base metal edge of the heat affected zone implies that an aging or solutioning response is induced in the base metal by the weld thermal cycle at the approach of recrystallization. This is most likely an interstitial effect realized as a result of low interstitial solubility in tungsten. A post weld stress relief of 1 hour at 2560°F (1400°C) proved marginal in improving weld ductility. Stress relief bend test data is included along with the as-welded data in Figure 5 for welds No. 1, 4, and 10.

Unalloyed Tungsten, Electron Beam Welding

Weld parameters for the electron beam welds in tungsten sheet are given in Table 3. Weldability was poor both as a result of brittle cleavage occuring during welding at higher

TABLE 2. Unalloyed Arc Cast Tungsten Sheet, TIG Weld Record

Weld No.	Type (1)	Clamp Spacing (inch)	Speed (ipm)	Current (amps)	Pre-Heat (°F)	Weld Width Top/Bottom (inch)	Q Kilojoules (per inch)	Comments - Visual, Dye Penetrant and Radiographic Inspection
1	Butt	3/8	7.5	155	--	.160/.140	21.10	Good Weld
2	BOP	3/8	7.5	163	550	.190/.175	22.15	Good Weld
3	Butt	3/8	7.5	115	--	.100/.040	15.62	Centerline crack, 1-1/2" long
4	BOP	3/8	7.5	121	550	.115/.050	16.45	Good Weld
5	Butt	3/8	15	176	--	.170/.150	11.90	One transverse (weld + Haz) crack
6	BOP	3/8	15	184	550	.200/.190	12.52	Good Weld
7	BOP	3/8	15	158	--	.140/.115	10.75	Good Weld
8	BOP	3/8	15	147	550	.130/.095	10.00	Good Weld
9	Butt	3/8	30	235	550	.180/.170	7.95	Propagated crater crack + Trans.(weld + Haz) crack.
10	Butt	3/8	30	220	--	.135/.100	7.45	Propagated crater crack + trans.(weld + Haz) crack.

(1) Fusion butt weld or bead-on-plate (BOP)

Astronuclear Laboratory

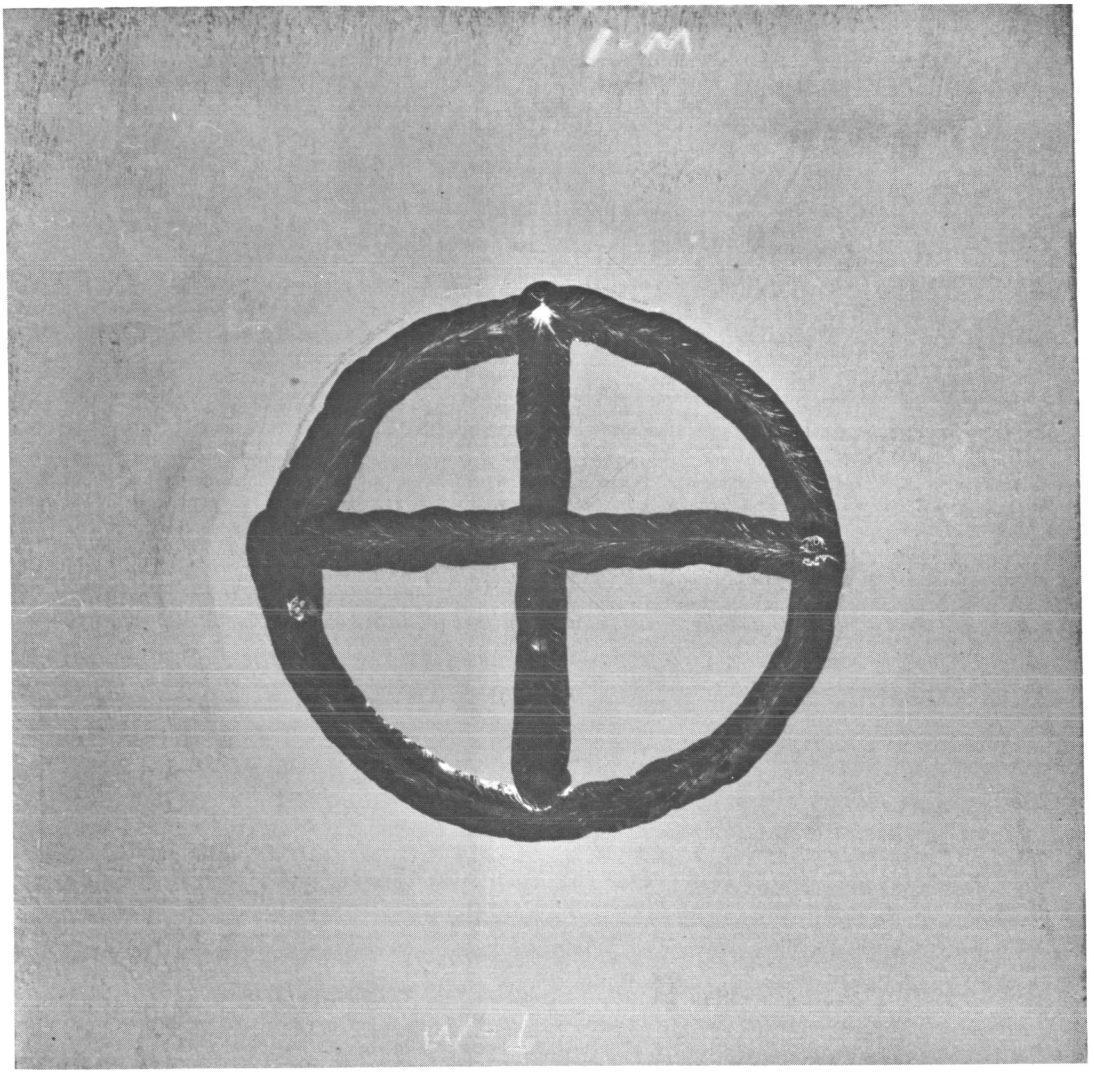
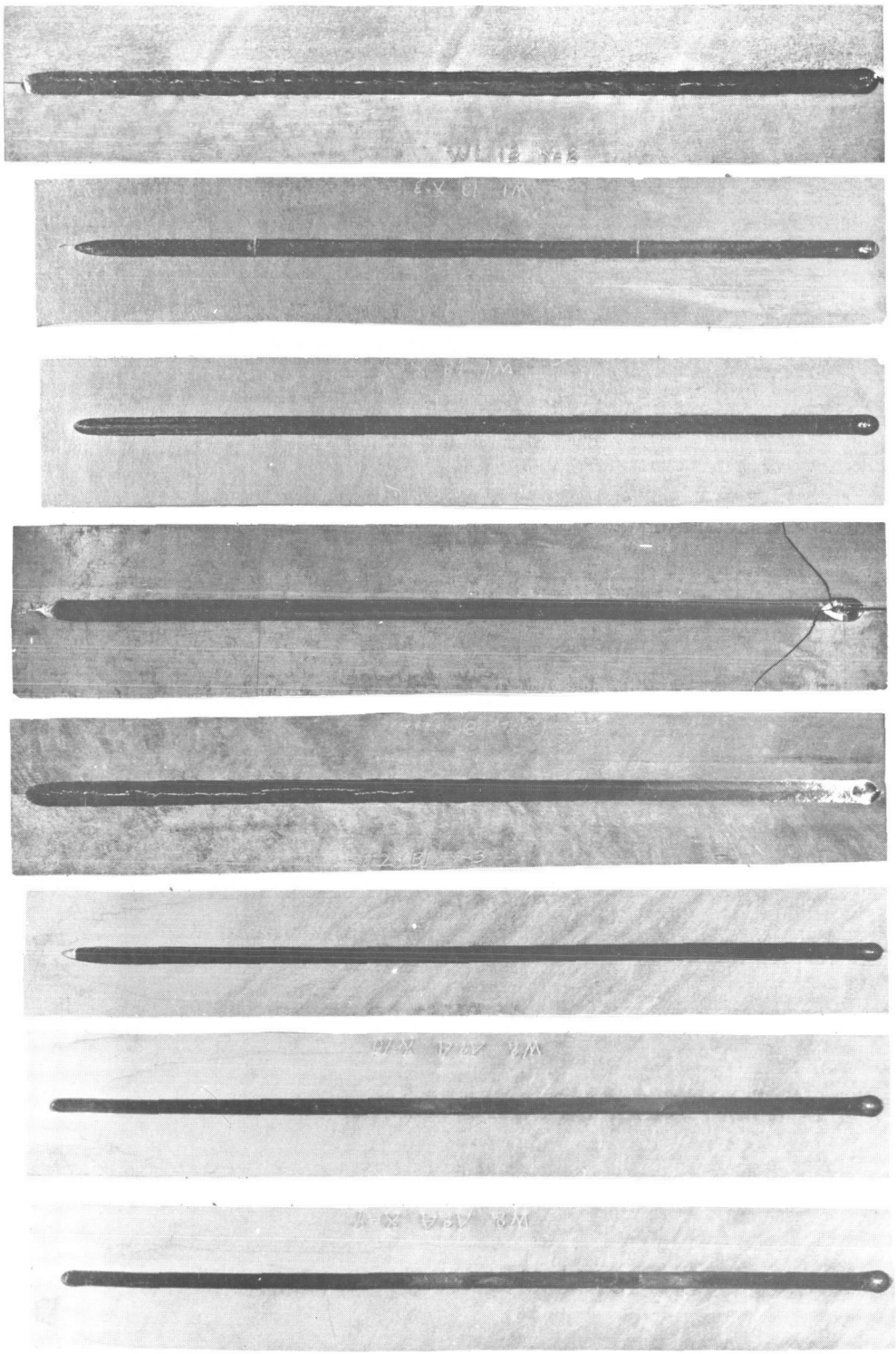




FIGURE 3 - Bead-on-Plate Patch Test of Unalloyed Tungsten



W, Weld No. 1
155 Amp at 7.5 ipm
21.1 Kilojoule/inch
No preheat.

W, Weld No. 8
147 Amp at 15 ipm
10.0 Kilojoule/inch
550°F preheat.

W, Weld No. 7
158 Amp at 14 ipm
10.75 Kilojoule/inch
No preheat.

W, Weld No. 10
220 Amp at 30 ipm
7.45 Kilojoule/inch
No preheat.

W-25Re, Weld No. 2
109 Amp at 7.5 ipm
14.83 Kilojoule/inch
450°F preheat.

W-25Re, Weld No. 7
102 Amp at 15 ipm
6.93 Kilojoule/inch
No preheat.

W-25Re, Weld No. 11
95 Amp at 3 ipm
32.30 Kilojoule/inch
No preheat.

W-25Re, Weld No. 12
90 Amp at 3 ipm
30.60 Kilojoule/inch
4550°F preheat.

FIGURE 4 - Typical TIG Butt Welds in Unalloyed Tungsten and W-25Re Sheet

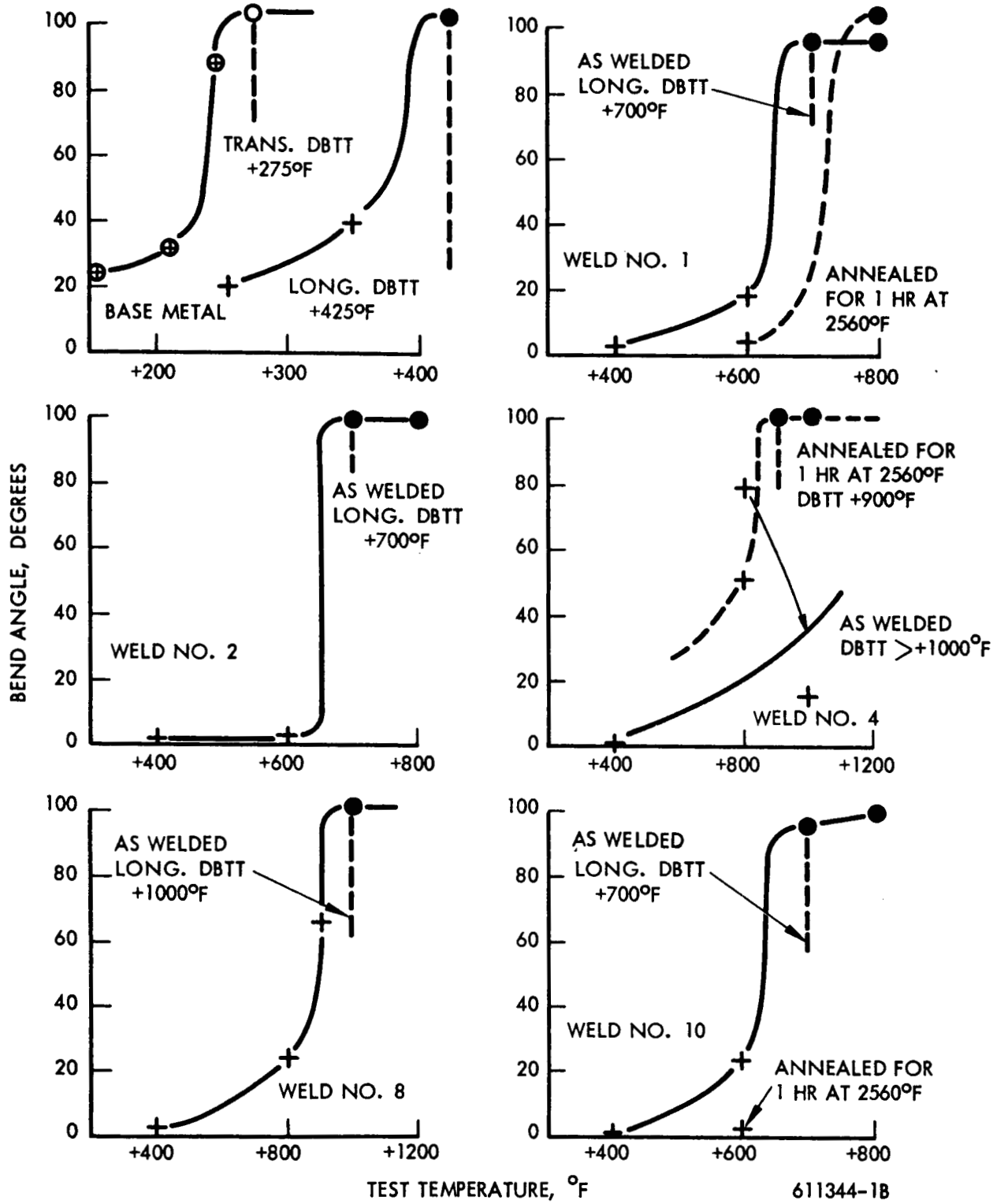
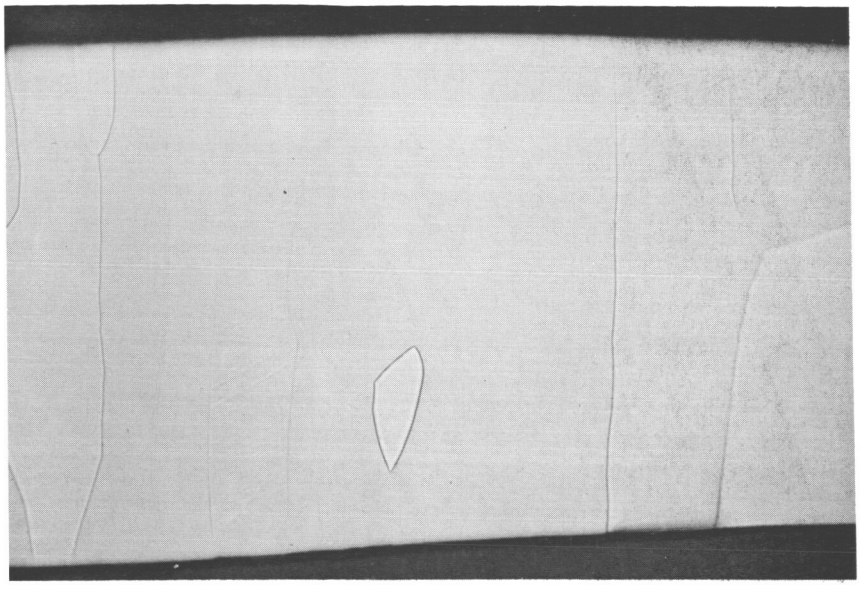
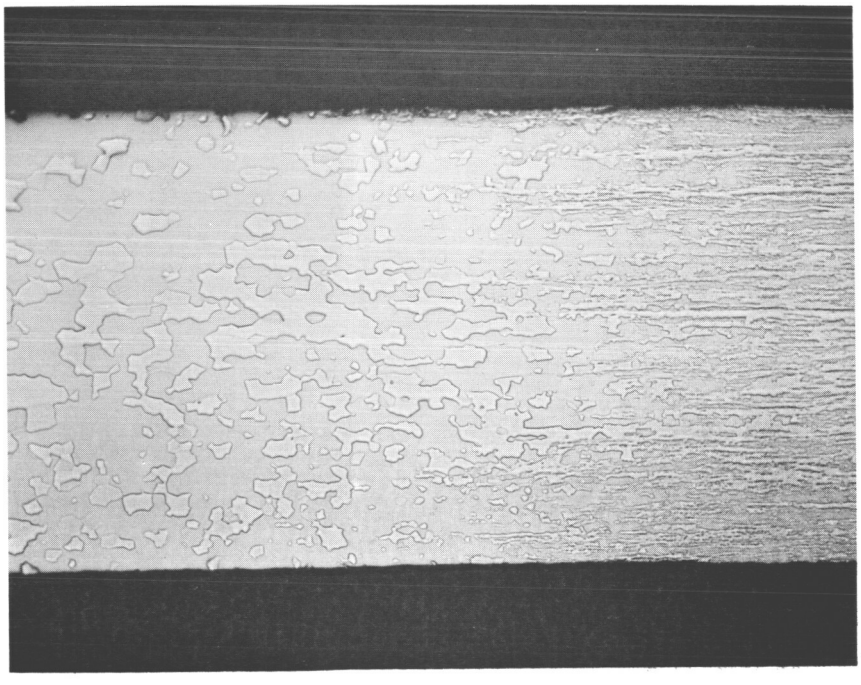


FIGURE 5 - Unalloyed Tungsten Sheet, Base Metal and TIG Weld Bend Test Results (4t Bend Radius)



13,582 Weld Structure 80X



13,582 Heat Affected Zone - Base Metal Structure 80X

FIGURE 6 - TIG Weld Structure in Unalloyed Tungsten, Weld No. 1, Table 2 (Welded at 7.5 ipm Without Preheat)

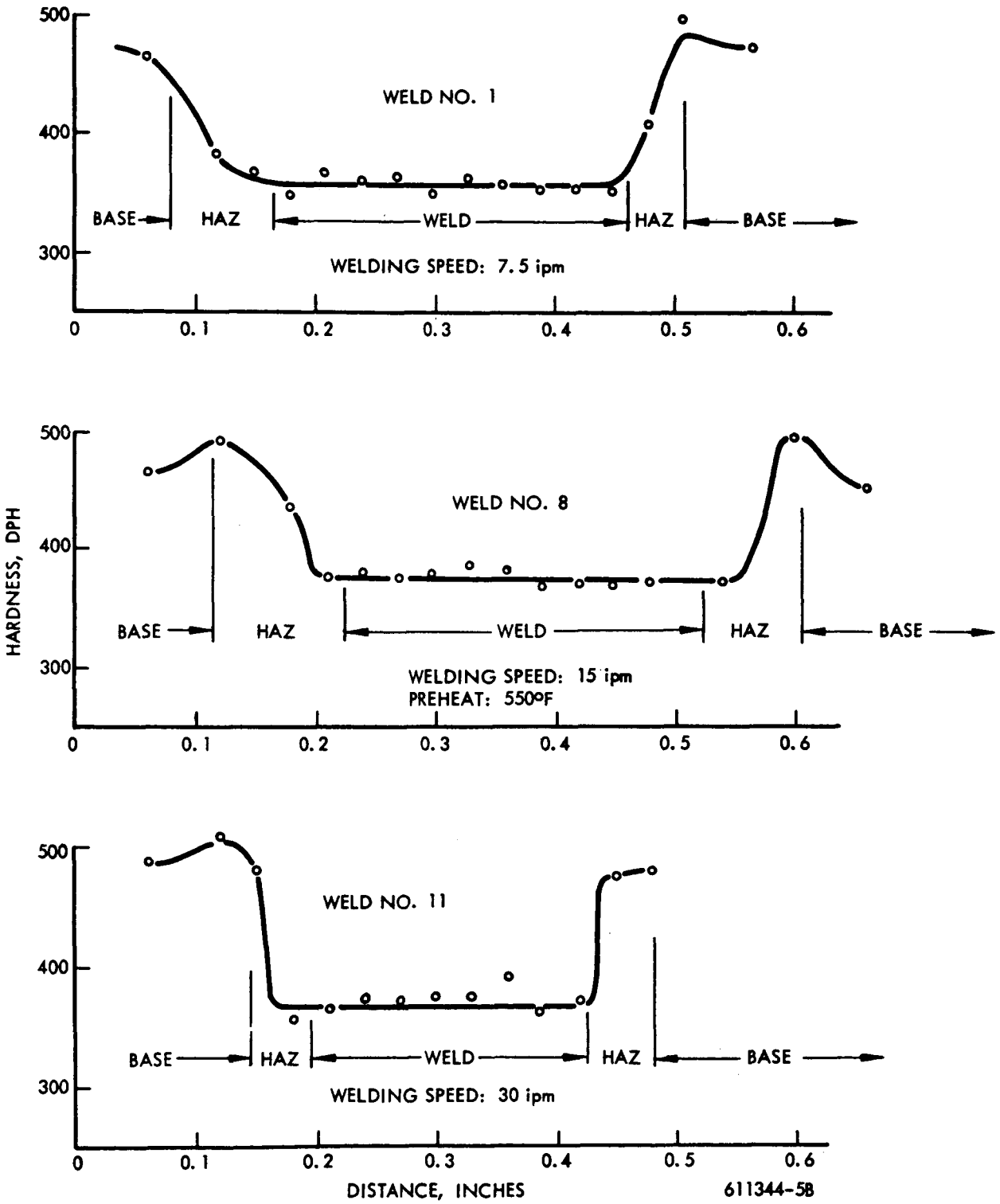


FIGURE 7 - Hardness Traverses of TIG Welds in Unalloyed Tungsten

TABLE 3. Unalloyed Arc Cast Tungsten Sheet, E. B. Weld Record

Weld No.	Speed (ipm)	Deflection (inches)	Current (Ma)	Chill Spacing (inches)	Power (Watts)	Watt-Sec. (Per inch)	Weld Bead Width (inches)		Vacuum (Torr)	Comments[3]
							Top	Bottom		
1	15	.050"-L	4.95	1/2	745	2980	.028	.012	4.4×10^{-6}	Bend tested
2[1]	15	.050"-T	4.40 / 4.80	1/2	660 / 720	2640 / 2880	.040	N.P.[2]	5.0×10^{-6}	Bend tested
3	25	.050"-L	4.95	1/2	745	1800	.025	N.P.[2]	4.4×10^{-6}	Bend tested
4	15	.050"-L	5.40	3/16	810	3240	.025	.015	4.4×10^{-6}	Bend tested
5	25	.050"-L	5.40	3/16	810	1940	.022	.010	4.4×10^{-6}	Bend tested
7	50	.050"-L	6.60	1/2	990	1190	.017	.015	5.0×10^{-6}	
8	100	.050"-L	7.80	1/2	1170	700	.017	.010	5.0×10^{-6}	
9	100	Zero	7.20	1/2	1080	650	.015	.010	5.0×10^{-6}	
10	15	.050"-T	5.20	3/16	780	3120	.040	.030	5.0×10^{-6}	Bead on Plate
11	50	.050"-L	7.20	3/16	1080	1300	.020	.020	5.0×10^{-6}	
12	100	.050"-L	8.50	3/16	1270	760	.020	.020	5.0×10^{-6}	Bead on Plate
13	100	Zero	7.80	3/16	1170	700	.015	.012	5.0×10^{-6}	Bead on Plate

(1) Rewelded because of lack of penetration on first pass.
(2) Bottom delaminated and bulged, no visible fusion.
(3) All welds defected as per dye penetrant.

speeds and because of a general underside delamination problem associated with this process. The delaminations occurred, as shown in the microstructure of Figure 8, on all welds. Cleavage cracking occurred in a number of characteristic modes as shown in Figure 9. In this figure cleavage cracks are shown for weld No. 3 (centerline crack), No. 4 (transverse), No. 7 (full section transverse, centerline, and arrested transverse), and Nos. 10 and 12 (peculiar "X" pattern arrested cleavage). The severity of weld cracking increased with welding speed. The numerous centerline defects in Figure 9 are caused by the typical root delaminations.

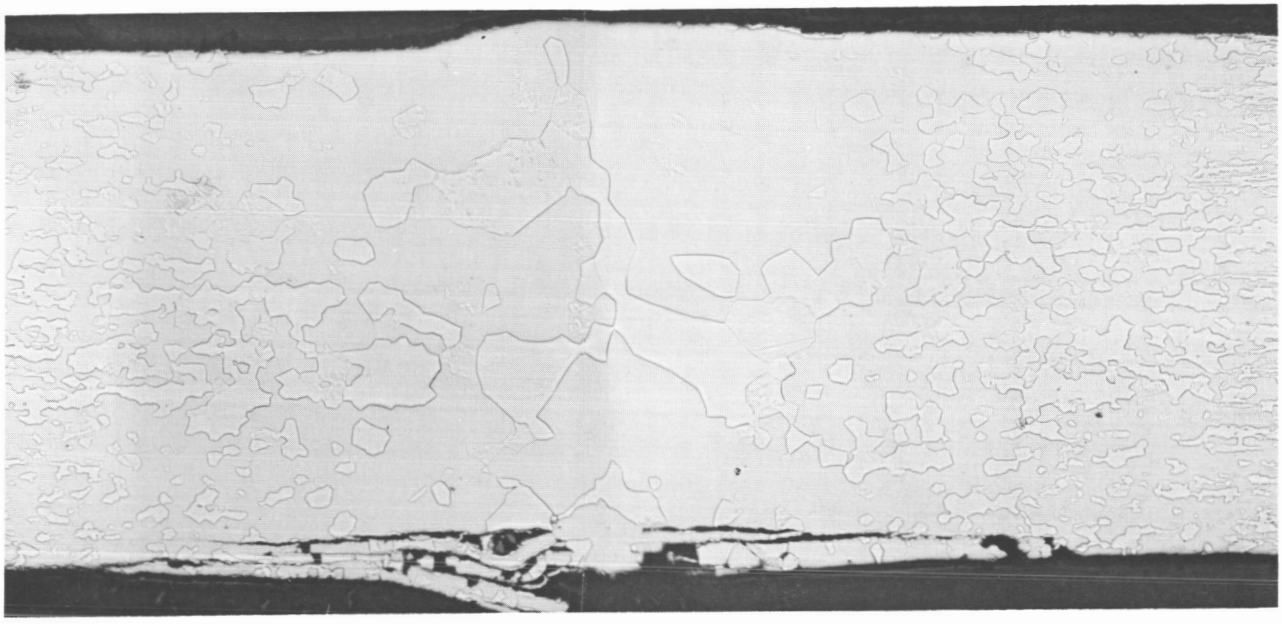
Transition temperature using 4t face bend tests, Figure 10, were in the +800 to $\geq$+ 1000°F temperature range. Only five welds of this group were suitable for bend testing.

W-25Re Sheet, Gas Tungsten Arc Welding

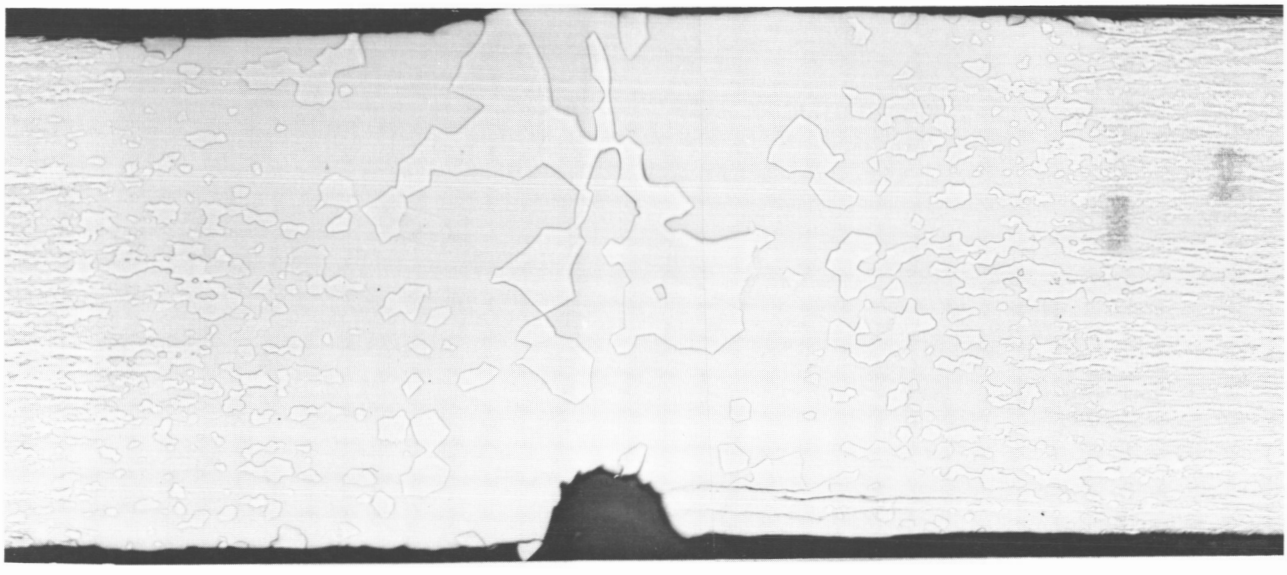
Weld parameters employed in evaluating this alloy and weld inspection results are listed in Table 4. As can be seen, welding became increasingly difficult with higher welding speeds. Transverse arrested cracks (weldand heat affected zone only) occurred in one 15 ipm weld and in all three 30 ipm welds. One 7.5 ipm weld contained a centerline crack which may have been a hot tear as was observed earlier in welding patch tests.[4] This alloy, like unalloyed tungsten, can be welded but with difficulty.

Bend specimens were cut from sound welds or apparently sound sections of defective welds. Bend test results are plotted individually in Figures 11 and 12. Bend transition temperatures varied from + 600°F to $>$ + 1000°F. The effect of weld parameters on weld ductility in this alloy is described by the summary presentation of Figure 13*. The data

*NOTE: For the purpose of data interpretation the bend transition temperature is defined as the temperature below which ductility is severely impaired as opposed to the lowest "zero defect" 90° bend temperature. This approach is technically sensible and in this program has provided more rational consistent interpretations. Testing is complicated to the extent that load deflection curves must be generated during a test to assure termination of the test at crack initiation (which may occur in the base, weld or heat affected zone).

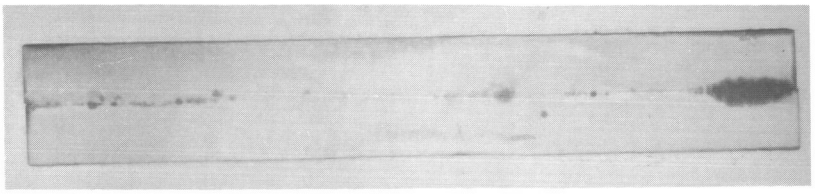


13,595 Weld No. 1 2.98 Kilojoules/inch at 15.6 ipm 80K

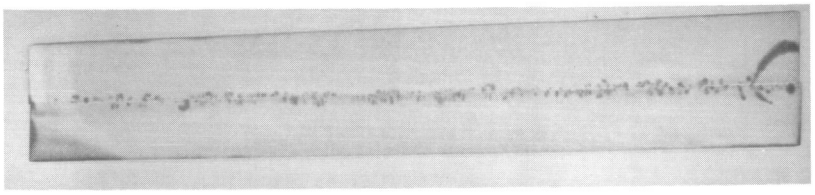


13,596 Weld No. 4 3.24 Kilojoules/inch at 15 ipm 80X

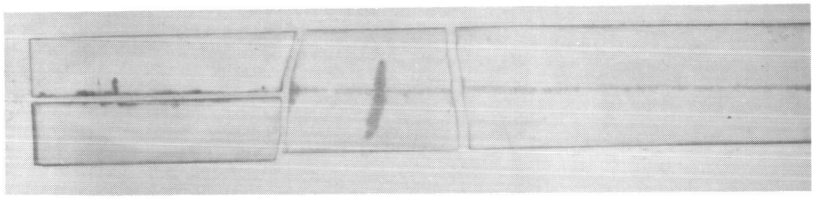
FIGURE 8 - Typical Sections of Electron Beam Welds in Unalloyed Tungsten



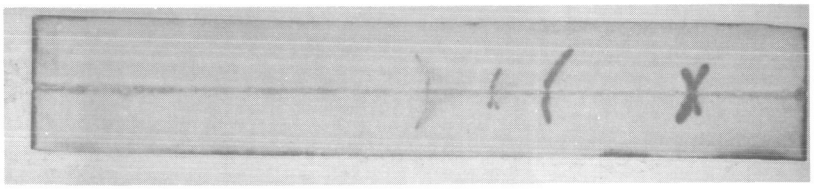
Weld No. 1
Speed - 15 ipm
2.98 Kilojoules/inch



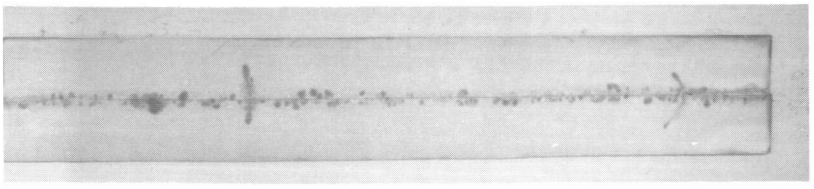
Weld No. 4
Speed - 15 ipm
3.24 Kilojoules/inch



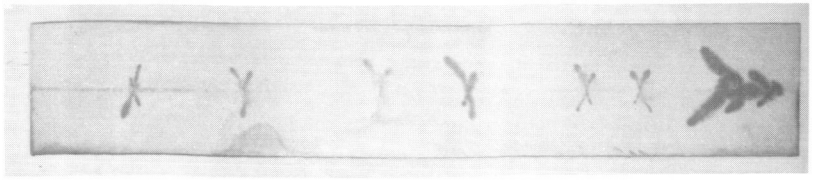
Weld No. 7
Speed - 50 ipm
1.19 Kilojoules/inch



Weld No. 10
Speed - 15 ipm
3.12 Kilojoules/inch



Weld No. 11
Speed - 50 ipm
1.30 Kilojoules/inch



Weld No. 12
Speed - 100 ipm
0.76 Kilojoules/inch

FIGURE 9 - Typical Dye-Penetrant Results of Electron Beam Welds in Arc Cast Unalloyed Tungsten Sheet

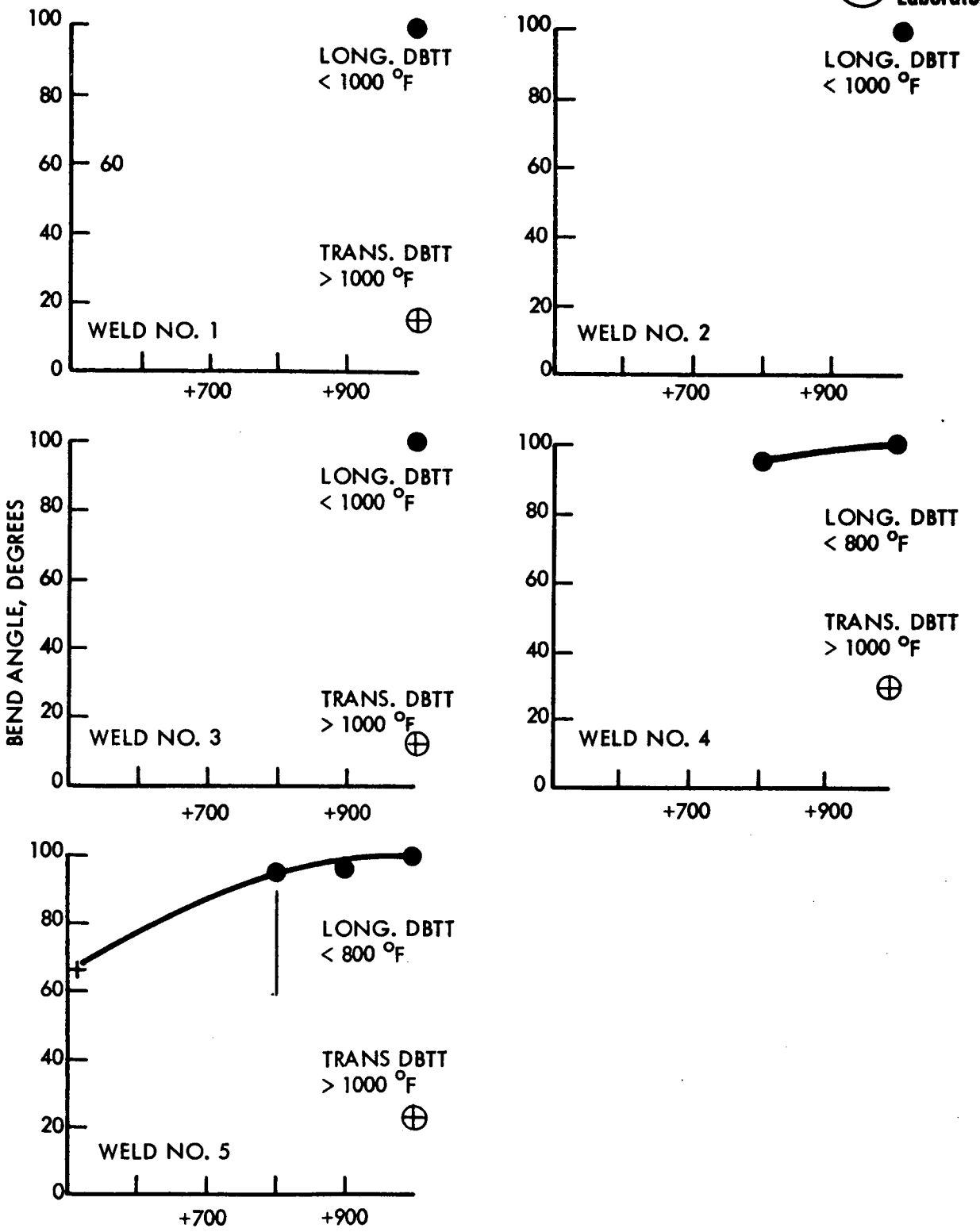


FIGURE 10 - Unalloyed Tungsten Sheet, EB Weld Bend Test Results (4t Bend Radius)

TABLE 4. W-25 Re Sheet, TIG Weld Record

Weld No.	Type (1)	Clamp Spacing (inch)	Speed (ipm)	Current (amps)	Pre-Heat (°F)	Weld Width Top/Bottom (inch)	Q Kilojoules (per inch)	Comments - Visual, Dye Penetrant and Radiographic Inspection
1	Butt	3/8	7.5	121	--	.170/.150	16.45	Good weld
2	Butt	3/8	7.5	109	450	.180/.170	14.83	Centerline weld crack 3" long
3	Butt	3/8	7.5	100	--	.150/.110	13.60	Good weld
4	Butt	3/8	7.5	83	550	.110/.055	11.29	Good weld
5	Butt	3/8	15	139	--	.180/.160	9.44	Three transverse cracks thru weld + Haz
6	Butt	3/8	15	131	450	.170/.150	8.90	Good weld
7	Butt	3/8	15	102	--	.120/.075	6.93	Good weld
8	Butt	3/8	30	204	--	.185/.160	6.93	Six transverse cracks thru Weld + Haz
9	Butt	3/8	30	185	450	.180/.160	6.28	Five transverse cracks thru Weld + Haz
10	BOP	3/8	30	147	550	.125/.110	5.00	Four transverse cracks thru Weld + Haz
11	BOP	3/8	3	95	--	.150/.110	32.30	Good weld
12	BOP	3/8	3	90	550	.150/.120	30.60	Good weld

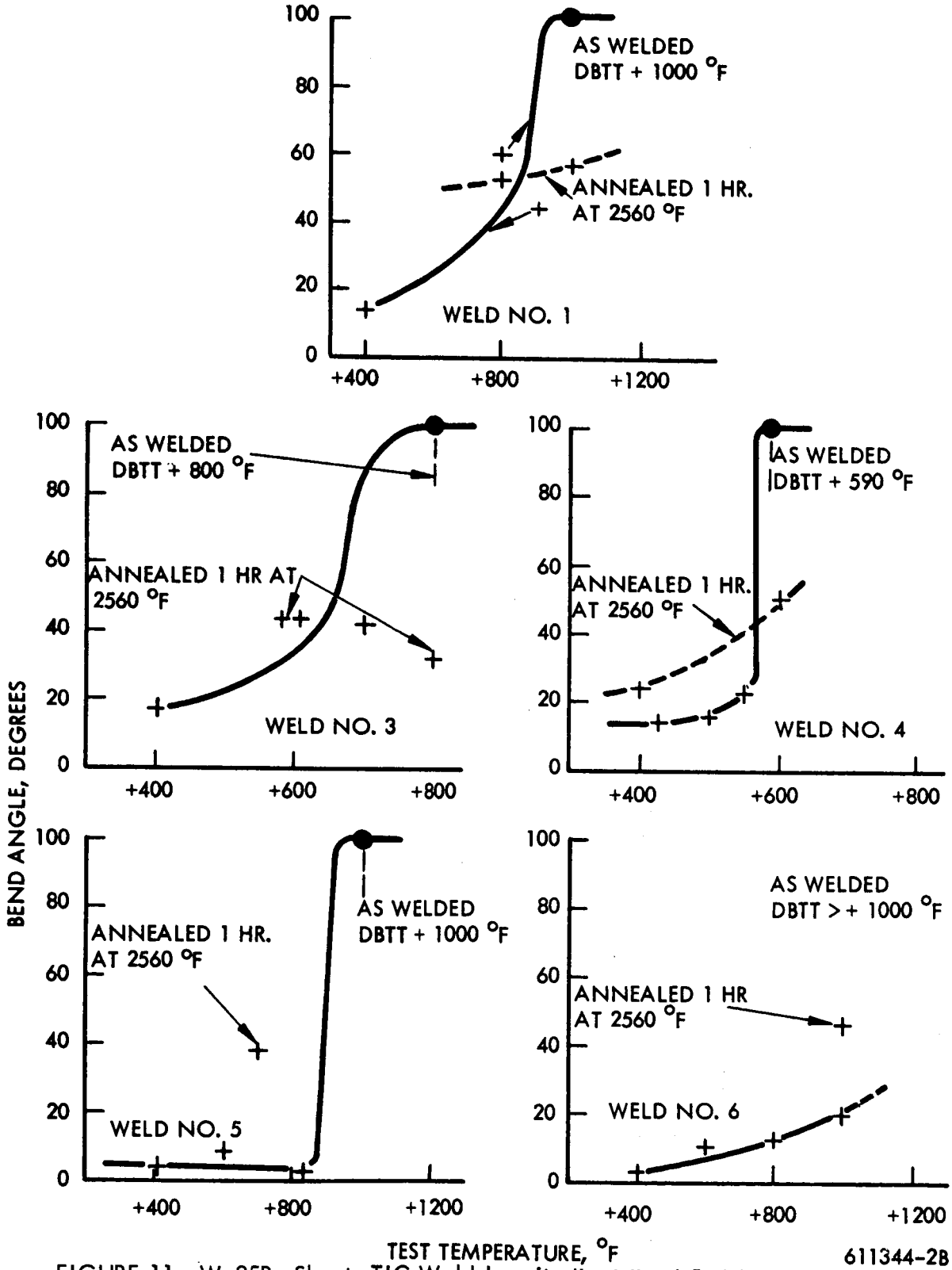


FIGURE 11 - W-25Re Sheet, TIG Weld Longitudinal Bend Test Results (4t Bend Radius)

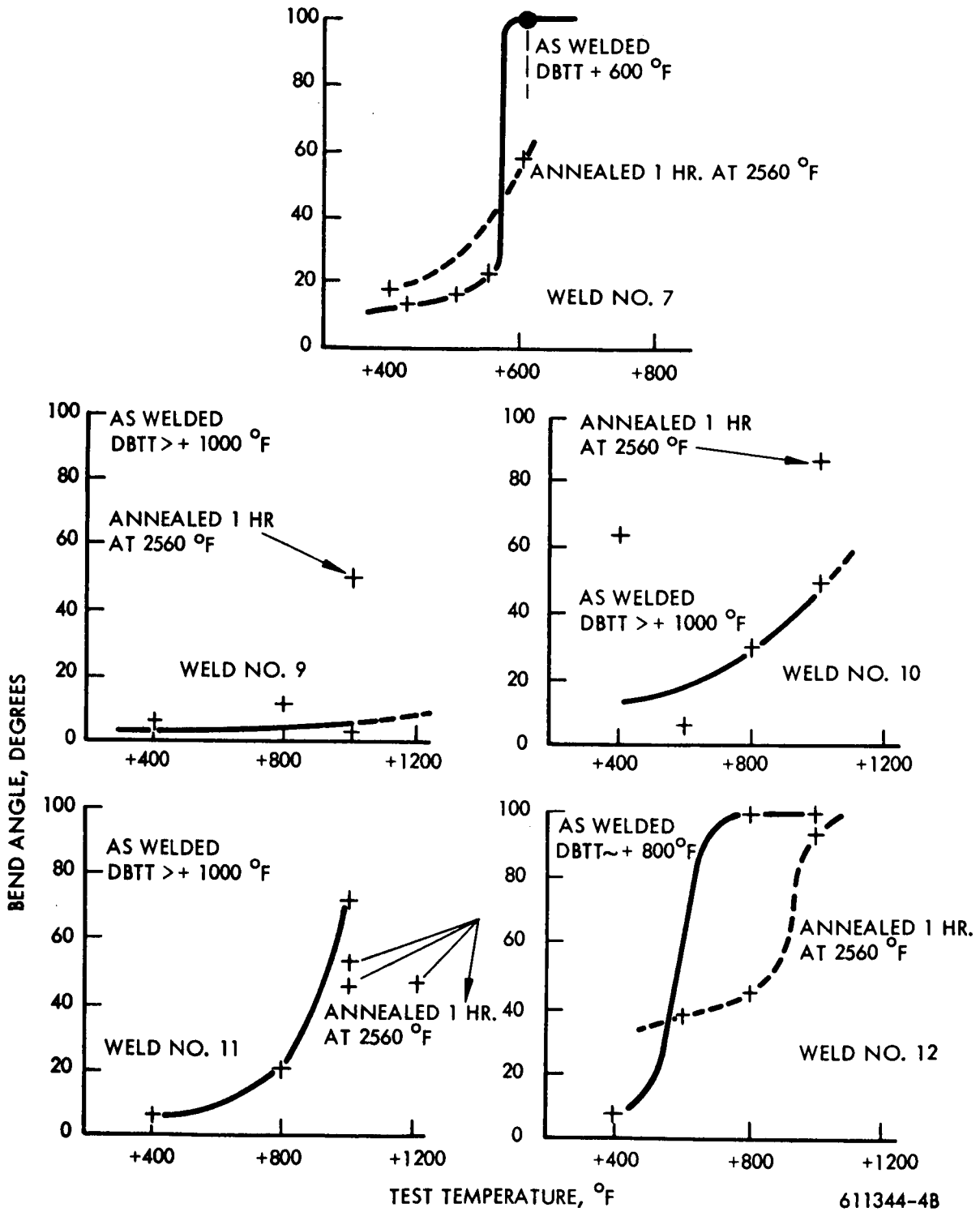


FIGURE 12 - W-25Re Sheet, TIG Weld Longitudinal Bend Test Results (4t Bend Radius)

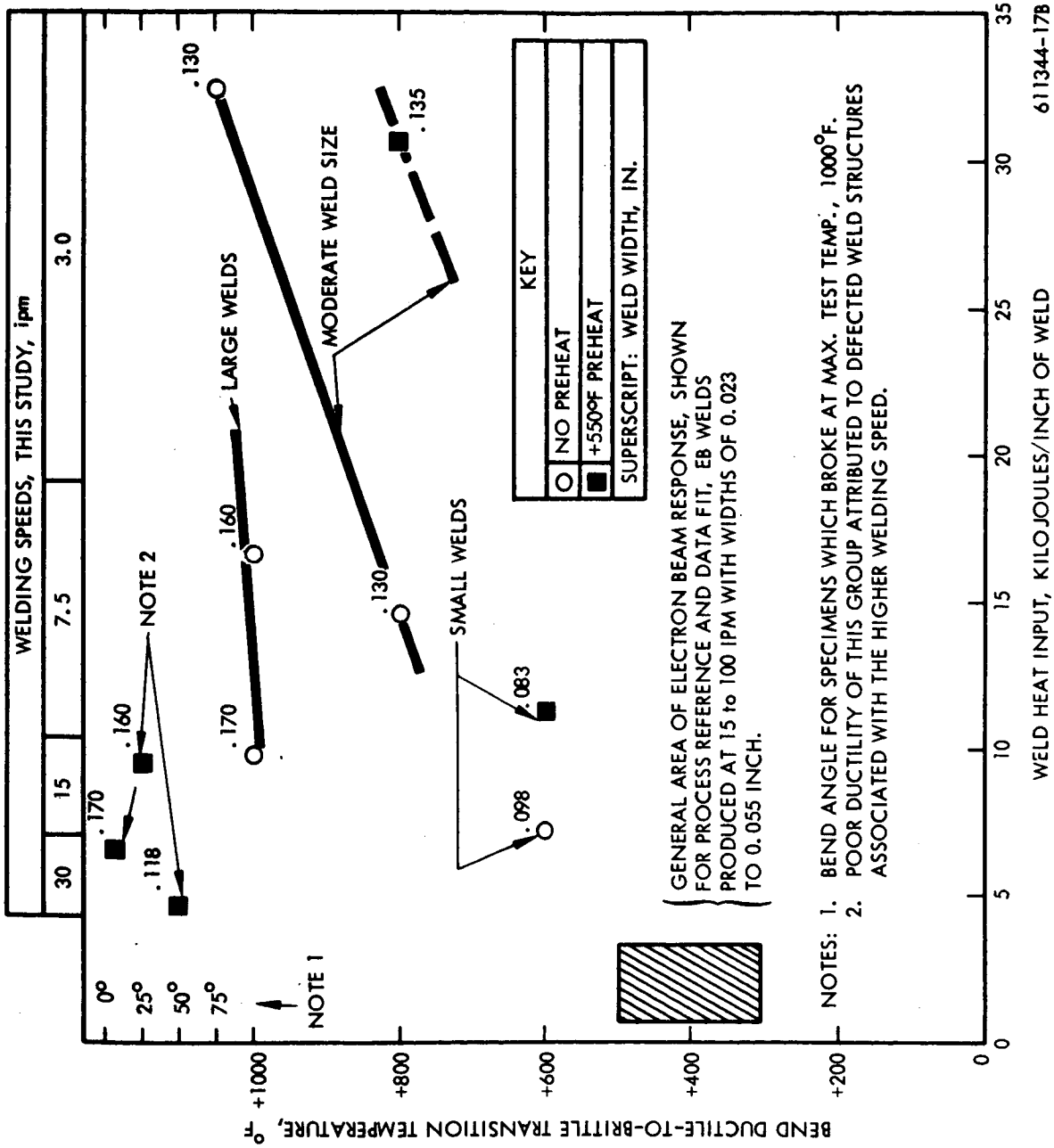


FIGURE 13 - The Effect of Weld Parameters on Ductility of Gas Tungsten Arc Welds in W-25Re Alloy Sheet

provide a reasonably consistent trend which relates the dependent variables affecting weld thermal cycles (heat input per unit weld length, weld size, preheat and weld speed) to ductility. An overall trend of improved ductility with decreased unit length heat input is apparent. Decreased heat input is achieved with decreased weld size and/or higher welding speeds for any one process, or it can be further decreased, as shown,by employing the electron beam welding process. The ductility of electron beam welds demonstrates excellent correlation with the heat input trend associated with gas tungsten arc welding. The selection of welding parameters must naturally be consistent with good weldability. In this respect, an observed trend towards less weldability at higher speeds is reflected in decreased ductility in several welds which presumably results from defected structures. Preheating appears to have a beneficial effect on weld ductility but not on weldability. As with unalloyed W, a post-weld stress relief of one hour at 2560°F(1400°C) is marginal in improving ductility (Figures 11 and 12).

Microstructures and hardness traverses of the W-25Re gas tungsten arc welds are shown in Figures 14 through 16. Significant differences in hardness of weld structures were not observed, Figure 14. Welds are about 100 DPH softer than the stress relieved base metal. The W-25Re welds are about 50 DPH harder throughout than equivalent welds in unalloyed W. A texturing effect is generally apparent in the weld area producing a slightly harder center area. As in W, the heat affected zone tends to have a slightly increased hardness over base metal in an area directly adjacent to unaffected base metal.

An interesting ductility/weldability correlation with microstructure was observed. Weld ductility and weldability were less for welding conditions under which twinning occurred in the cast weld structure. This is shown in Figures 15 and 16. The preheated 7.5 ipm weld did not twin, whereas the non-preheated 7.5 ipm weld did twin and also had poorer ductility, Figure 15. Increased twinning, and less ductility, was observed in the 3 ipm, no preheat weld. Increased weld speeds, 15 and 30 ipm, even with preheat had twinned structures and less ductility, Figure 16. Variability of twinning is probably indicative of variability of weld induced residual strain since twinning is a strain associated phenomena. Hence, these results imply that the observed variability in weld ductility in this system is most likely

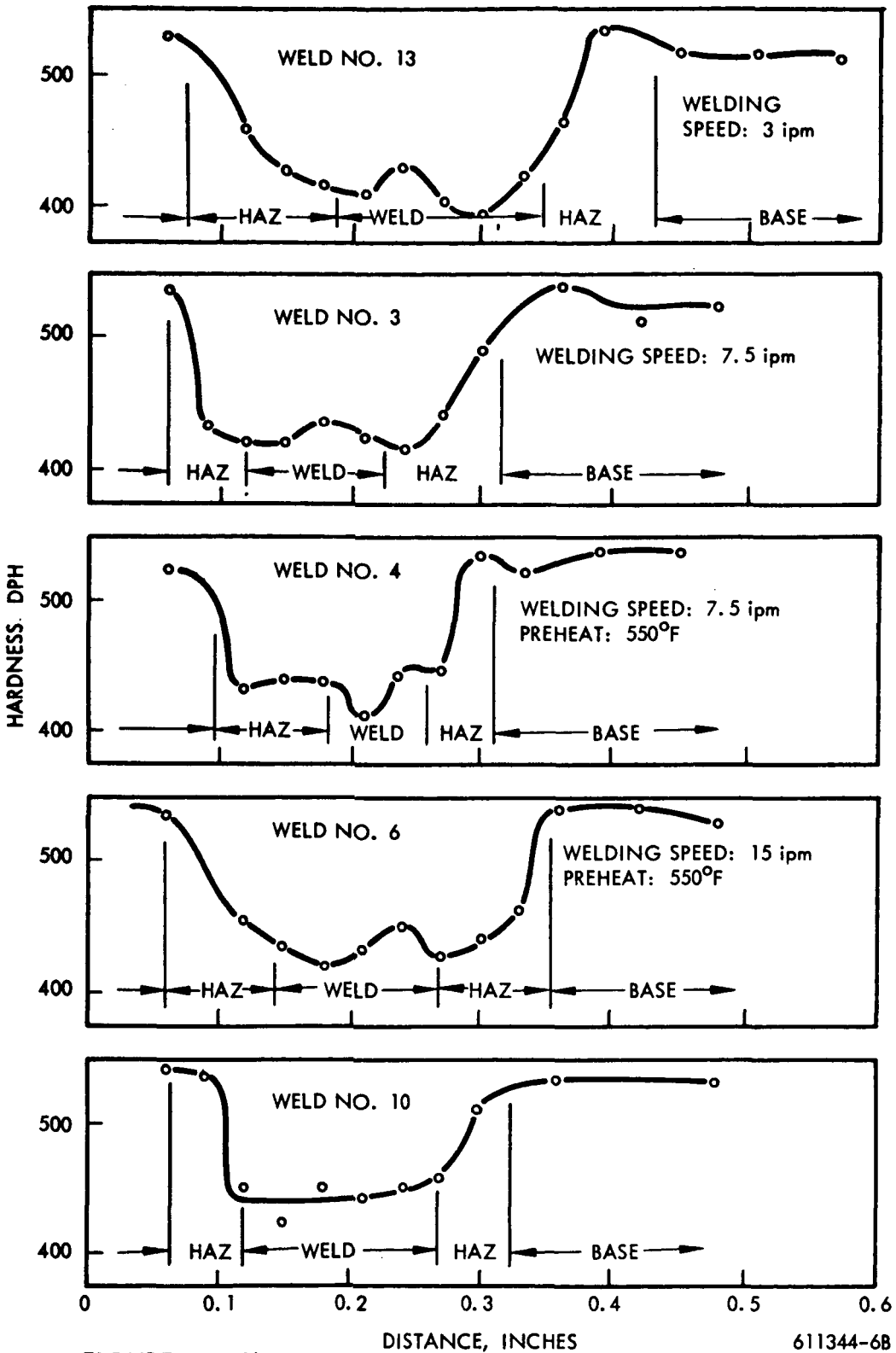
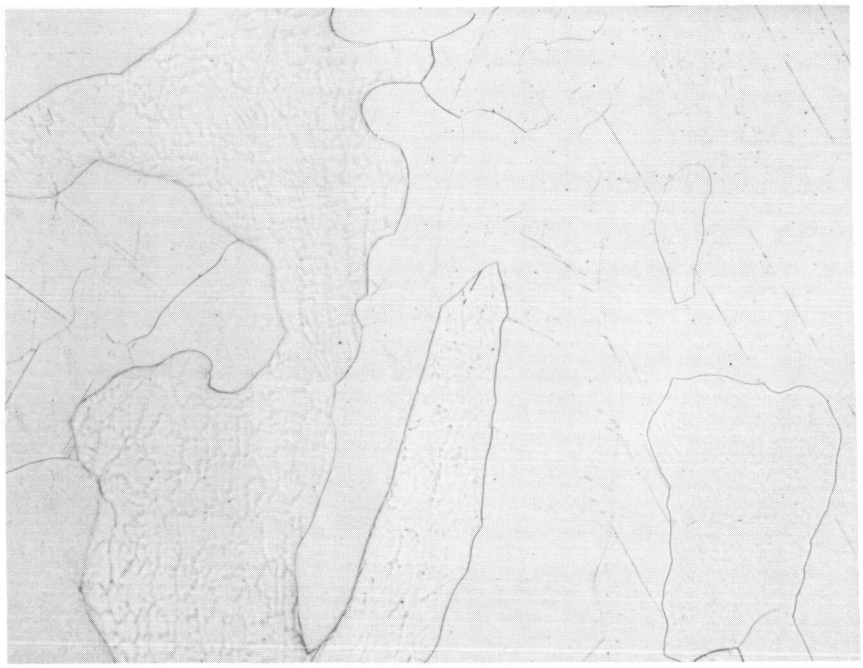
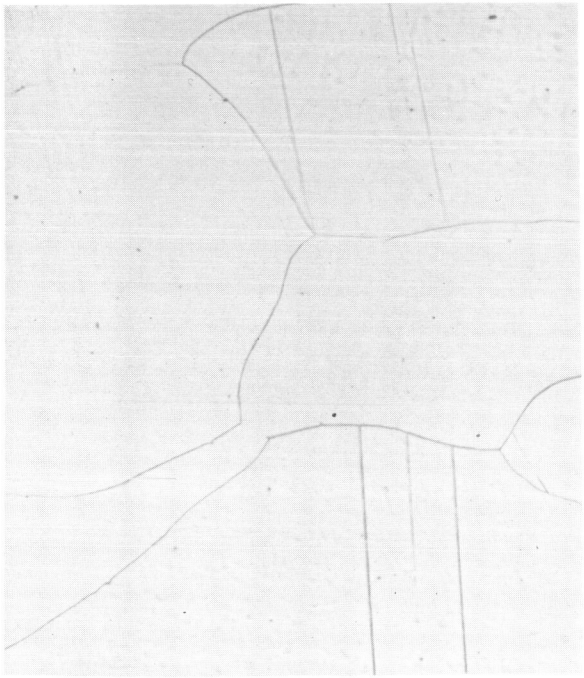


FIGURE 14 - Hardness Traverses of TIG Welds in W-25Re Sheet



13,592 Weld No. 11 100X
3 ipm, No Preheat
32.3 Kilojoules/inch



13,587 Weld No. 1; 7.5 ipm 300X
No Preheat; 16.45 Kilojoules/inch



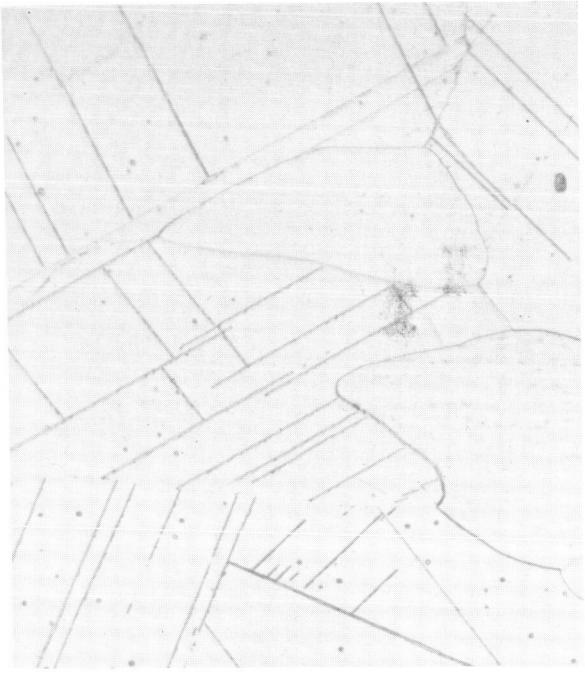
13,589 Weld No. 4; 7.5 ipm 300X
Preheated; 11.29 Kilojoules/inch

FIGURE 15 - Photomicrographs of Cast Weld Area in Gas Tungsten Arc Welded W-25Re Sheet



13,590 Weld No. 6; 15 ipm 100X
Preheated; 8.9 Kilojoules/inch





13,591 100X 13,591 300X
Weld No. 9; 30 ipm; preheated; 6.28 Kilojoules/inch

FIGURE 16 - Photomicrographs of Cast Weld Area in Gas Tungsten Arc Welded W-25Re Sheet

related to the effect of weld parameters on stress distribution, as opposed to metallurgical structure.

Sylvania "A", Gas Tungsten Arc Welding

No satisfactory welds were produced in this alloy due to extreme brittleness. This alloy is apparently unweldable as illustrated by the results obtained, Figures 17 and 18, in the arc welding study. No metallographic or electron beam welding evaluation of this alloy was undertaken. Weld parameters are listed in Table 5.

B. EFFECT OF OXYGEN CONTAMINATION ON WELDABILITY

The effect of oxygen contamination on the weldability and thermal stability of three selected refractory metal alloys (FS-85, T-111 and T-222) is being evaluated as an additional phase to the overall weldability study. Although much information has been generated indicating the desirability and demonstrating the feasibility of maintaining low oxygen levels in refractory metal alloys, a measure of the oxygen tolerance of typical alloys was not available. And, whether contaminated slowly through long exposure at less than optimum conditions, (anticipated system lifetimes are over 10,000 hours), or contaminated in sudden bursts by component failures, some oxygen influenced changes in materials properties must be anticipated. Weldability was chosen as the basic measure of performance for two reasons. First, repair and modification operations requiring welding will certainly be needed for systems with operating lives measured in years. Second, the welding process, by generating a wide gamut of thermal histories, i.e., as-cast, solution treated, overaged, aged, etc., metal; provides a sensitive and realistic test for subtle changes in material properties. The scope of this alloy screening phase covered a broad range of oxygen contamination levels and temperatures spanning the range of service operating conditions, simulating actual hardware which is contaminated with oxygen and subsequently welded as in a repair or modification operation. Admittedly, as a screening study this evaluation inherently is incomplete and the short time tensile properties may be quite different from the response in long time testing. Additional work is in progress to determine the long time effects of aging on the response of welded

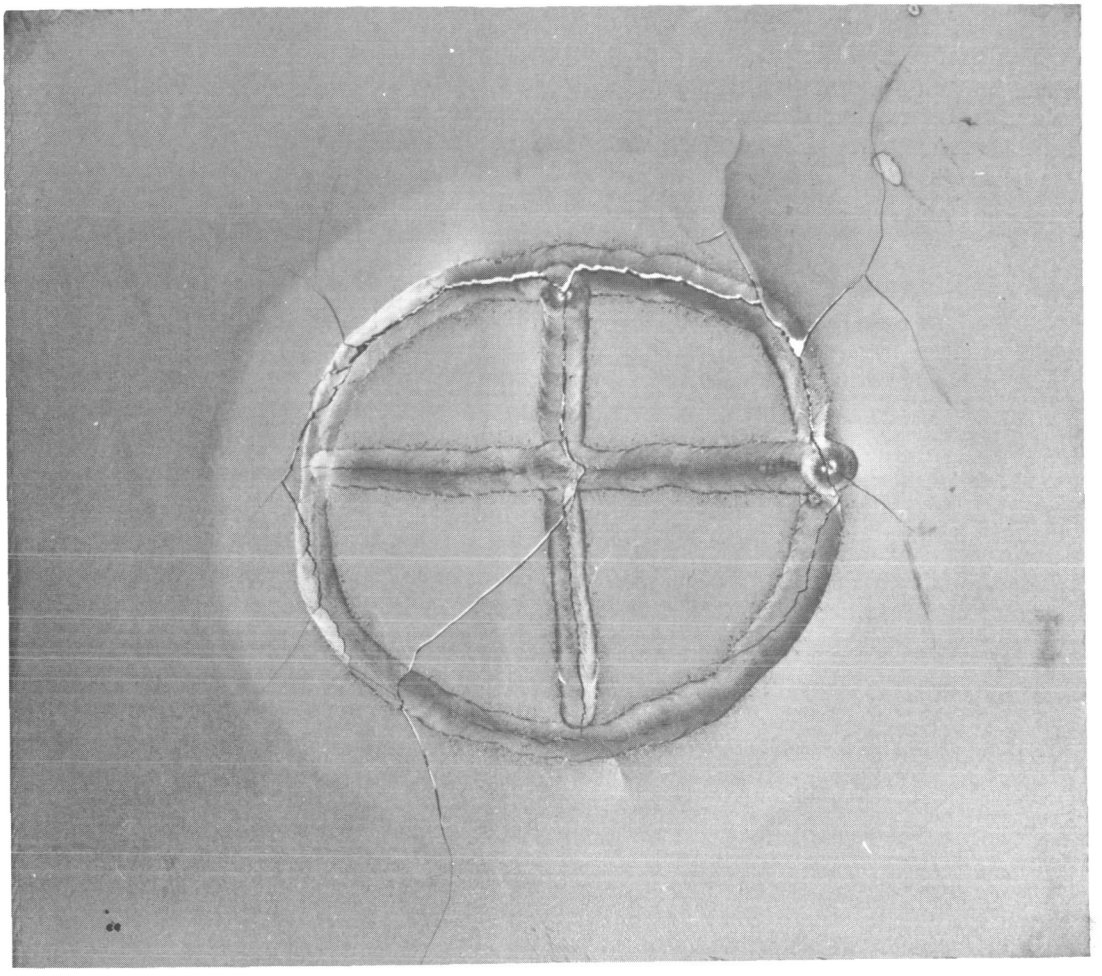
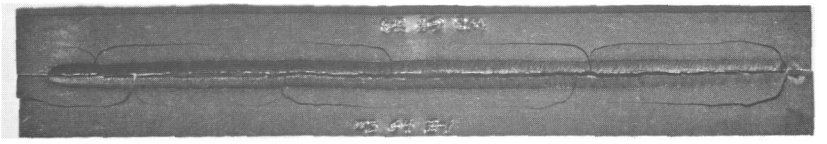
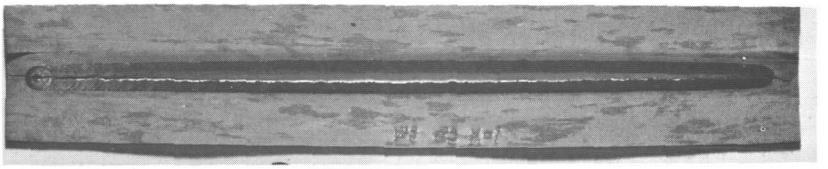


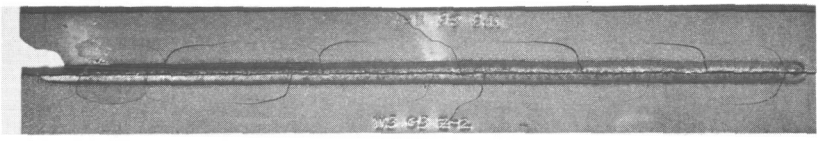
FIGURE 17 - Bead-on-Plate Patch Test of Sylvania "A"



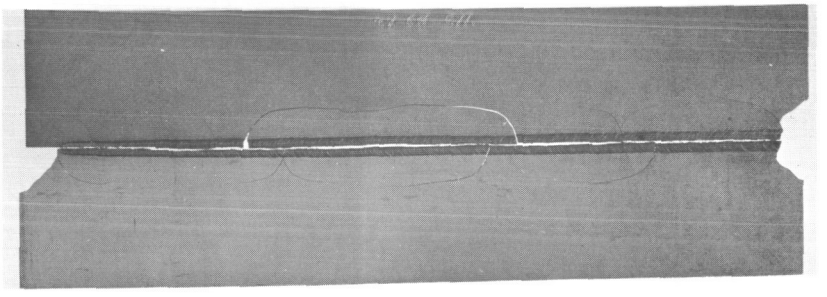
Weld No. 1 First Try; Preheated 550°F; 7.5 ipm 871-2



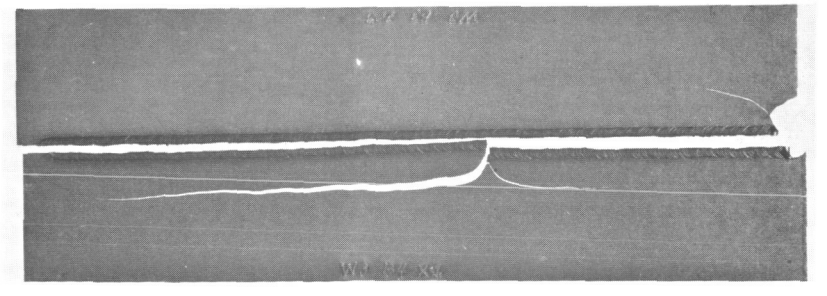
Weld No. 1 Second Try; Preheated 550°F; 7.5 ipm 871-2



Weld No. 2 No Preheat; 1.5 ipm; 119.8 Kilojoules/inch 871-2



Weld No. 3 No Preheat; 3 ipm; 44.2 Kilojoules/inch 6023



Weld No. 4 Preheated 550°F; 3 ipm; 42.5 Kilojoules/inch 6023

FIGURE 18 - Gas Tungsten Arc Butt Welds in Sylvania "A"

TABLE 5. Sylvania "A" Sheet, TIG Weld Record

Weld No.	Type	Clamp Spacing (inch)	Speed (ipm)	Current (amps)	Pre-Heat (°F)	Weld Width Top/Bottom (inch)	Q Kilojoules (per inch)	Comments - Visual, Dye Penetrant and Radiographic Inspection
1	Butt	3/8	7.5	163	550	--	--	Badly cracked
2	Butt	3/8	1.5	176	--	.170/.170	11.9	Badly cracked
3	Butt	3/8	3	130	--	.150/.140	44.2	Badly cracked
4	Butt	3/8	3	125	500	.170/.160	42.5	Badly cracked

and unwelded material to oxygen contamination. Gaseous oxidation with a low partial pressure of oxygen in helium carrier gas is being used to contaminate 0.035-inch alloy sheet. At the doping temperatures employed, from 800°F to 1100°F, and an oxygen partial pressure range of 10^{-1} to 1 Torr, an adherent oxide film is produced which is subsequently diffusion annealed at higher temperatures. The apparatus and process control are described in detail in a preceding report.[8] Figure 19 outlines the overall contamination program.

The initial phase of the program, screening three candidate alloys for tolerance to oxygen contamination, is completed with the presentation of tensile test data in this report. The degrading effects of oxygen contamination on both base and weld metal properties were measured by weld bend ductility tests, restrained welds in the form of patch tests, and transverse weld tensile tests at room temperature and three elevated temperatures. Five oxygen contamination levels were employed to follow sudden changes in response to oxygen contamination and four tensile test temperatures were evaluated to simulate service conditions. In review, the weld bend ductility results[9] indicated that both FS-85 and T-111 were tolerant to fairly high oxygen contamination levels (500,350 wt. ppm)* and T-222 was less tolerant showing a sharp loss in ductility at 200 wt ppm oxygen. The tensile test results have indicated a similar response with no marked deterioration in properties up to 500, 350 wt. ppm oxygen. At the higher oxygen contamination levels a loss in ductility as measured by a sharp decrease in tensile elongation was observed. It is significant to note that tensile and yield strength showed a steady increase with oxygen content at all test temperatures. Previous studies by Begley[10] and Ammon[11] indicated that oxygen additions had a mixed effect on the hardness and strength of columbium and tantalum; in some cases hardness was observed to decrease with oxygen content[9], apparently by removing Hf and Zr from solid solution. The loss of solid solution strengthening was not compensated by precipitation strengthening by the oxide phases. The oxygen additions were made by adding base metal oxides to the melt as

*NOTE: Alloys are compared at equivalent atomic ppm. Tantalum alloys were doped to lower weight ppm levels to adjust for differences in atomic weight. Hence, two contamination levels are indicated wherever the tantalum and columbium alloys are being referred to simultaneously.

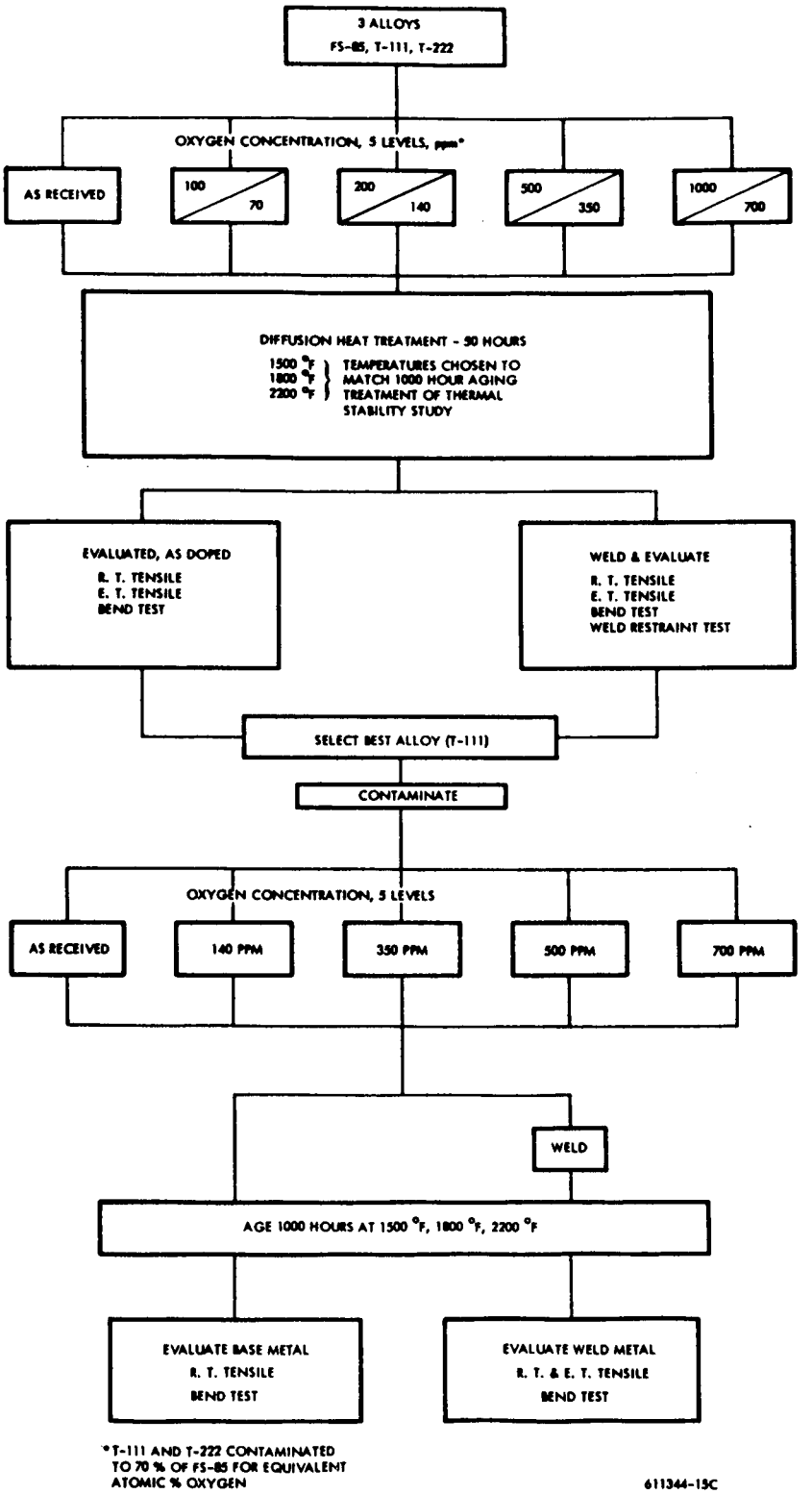


FIGURE 19 - Program Outline for Contaminated Alloy Weldability Evaluation

compared to the gaseous oxidation process used in the present study. Apparently, the form and distribution of the oxide phases is most important and the two methods of oxygen addition could produce quite different forms. The oxides observed by Ammon[11] were large and globular and recent evaluations of gaseous oxidized tantalum base alloys by Buckman and Goodspeed[12] indicate the oxygen to be present either in solution or as a fine coherent precipitate. Complementary hardness data shows an increase in hardness with oxygen content.

The highest oxygen levels, 1000, 700 wt ppm, produced a sharp loss in ductility resulting in a high mortality rate in the tensile specimens. Only one bonafide test was obtained for T-222, two specimens failed during machining and one failed in the grip hole during testing. T-111 and FS-85 fared better with one pin grip failure in T-111 and no specimen losses in FS-85.

Tensile Test Results

In presenting this large amount of tensile test data of transverse weld specimens of three alloys, five oxygen levels and four test temperatures, an attempt is made to generalize the data in terms of thermally controlled precipitation and diffusion reactions. The generalization is presented first as a summary by test temperature and is followed by a more direct data presentation for the three alloys.

Test Temperature Summary

The response of the three alloys to oxygen contamination may be summarized by grouping the alloys at the four different test temperatures. Since the alloys were oxygen contaminated at a maximum temperature of 1100°F, the higher temperatures experienced during tensile testing were of paramount importance in determining the form, distribution, and related strengthening effects of the oxygen contamination. Following the low temperature oxygen contamination process, the specimens were diffusion annealed for 50 hours at temperatures corresponding to subsequent test temperatures. One exception was the group of specimens destined for tensile testing at room temperature; these specimens were diffusion annealed at 1800°F and as a

result their structure and properties would be expected to be similar to specimens tested at 1800°F. Consequently, in attempting to generalize with respect to maximum thermal exposure, the 1500°F tensile specimens must be considered to have a lower overall thermal exposure than the room temperature tested specimens.

1500°F Tensile Test Temperature

After a 50 hour exposure at 1500°F, the oxygen contaminated material exhibited significant changes in base metal properties. At this temperature, FS-85 is more strongly affected than the tantalum base alloys, indicating more rapid diffusion or precipitation reactions for the columbium base alloy. A comparison of the yield strengths of the three alloys, Figures 20, 23, and 26, show nearly twice the percentage strength increase for FS-85 as T-111, from the uncontaminated oxygen level to the 500, 350 ppm oxygen level, the highest level for which a complete series of samples was available. In FS-85 the addition of oxygen moves the fracture location from the base metal to the weld and heat affected zone, Figure 37, and Table 8, whereas in the tantalum base alloys, the weakest area remains predominantly in the base metal. In FS-85, the weld structures ranging from cast metal in the weld to overaged structures at the edge of the heat affected zone, are weaker than the oxide strengthened base metal. The loss in ductility, as measured by tensile elongation, is most severe for FS-85, dropping from 15% to 5%, Figure 28. Fracture appearance is ductile for all oxygen levels in FS-85, and ductile up to the highest oxygen level in T-111 with no real fracture comparison available for T-222 at the highest oxygen level since the specimen failed through the pin grip, Figures 29, 33, and 37.

1800°F Tensile Test Temperature

The 1800°F testing and diffusion annealing temperature has emphasized the oxygen diffusion-precipitation reactions strengthening the tantalum base alloys. T-222 actually shows a significant increase in yield strength at 1800°F for the higher oxygen levels, Figure 23. FS-85, the columbium base alloy shows a general decrease in yield and tensile strength from 1500°F to 1800°F, Figure 26. At 1800°F, the tantalum base alloys show the same shift in fracture location with oxygen content as was observed in FS-85 at 1500°F; increasing oxygen

TABLE 6. Tensile Test Properties of T-111 at Five Oxygen Levels

Tensile Test Temp. (°F)	50-Hr. Diffusion Temp. (°F)	Contamination Level PPM O_2	Calculated[2] Total Oxygen Content	Specimen No.	Y. S. 0.2% Offset Psi x 10^3	Ultimate Stress Psi x 10^3	Elongation %	Fracture Location	Distance From weld Centerline (inches)
Room Temp.	1800	0	40	T1CU-3	75.3	86.6	19.5	Base[1]	1.00
		70	125	T1C4-1	62.7	85.2	14.0	HAZ[1]	0.12
		140	220	T1C3-1	85.3	96.0	9.0	HAZ[1]	0.16
		350	355	T1C1-3	88.5	99.0	3.5	HAZ[1]	0.12
		700	800	T1C2-2	87.6	94.1	2.0	HAZ[1]	0.12
1500	1500	0	40	T1CU-1	38.8	64.0	14.0	Base	0.47
		70	110	T1C4-2	40.9	66.8	14.0	Base	0.35
		140	210	T1C3-4	44.0	70.7	13.0	Base	0.47
		350	380	T1C1-2	50.6	70.6	8.0	Weld	0.05
		700	810	T1C2-1	56.5	72.8	5.0	Base	0.40
1800	1800	0	40	T1CU-4	33.9	57.3	15.0	Base	0.42
		70	110	T1C4-3	35.8	61.4	15.0	Base[1]	0.40
		140	225	T1C3-2	43.5	66.3	9.0	HAZ[1]	0.15
		350	370	T1C1-4	51.6	66.3	7.0	HAZ[1]	0.15
		700	810	T1C2-3	--	58.1	—Failed in Grip Hole—		
2200	2200	0	40	T1CU-2	29.0	42.4	24.0	Base	0.40
		70	125	T1C4-4	29.7	42.0	23.0	Base	0.55
		140	210	T1C3-3	31.8	44.3	22.0	Base	0.45
		350	380	T1C1-1	35.5	46.6	22.0	Base	0.42
		700	810	T1C2-4	41.5	48.9	16.0	Weld	0.01

(1) Heat Affected Zone
(2) Based on weight gain following diffusion annealing and as received oxygen content of 40 ppm.

TABLE 7. Tensile Test Properties of T-222 at Five Oxygen Levels

Tensile Test (°F)	50-Hr. Diffusion Temp. (°F)	Contamination Level PPM O_2	Calculated[2] Total Oxygen Content	Specimen No.	Y. S. 0.2% Offset Psi x 10^3	Ultimate Stress Psi x 10^3	Elongation %	Fracture Location	Distance From Weld Centerline (inches)
Room Temp.	1800	0	75	T3CU-2	73.8	85.2	12.0	Base	0.90
		70	165	T3C4-1	82.8	94.2	11.0	Base	0.25
		140	230	T3C3-2	74.4	102.9	5.0	HAZ[1]	0.15
		350	360	T3C1-2	98.7	106.6	3.0	HAZ[1]	0.13
		700	—No test specimen fractured during machining—						
1500	1500	0	75	T3CU-1	40.3	61.5	10.0	Base	0.40
		70	250	T3C4-2	42.7	66.0	10.0	Base	0.45
		140	270	T3C3-1	44.7	69.7	11.0	Base	0.42
		350	370	T3C1-4	49.6	75.5	11.0	Base	0.40
		700	950	T3C2-3	58.2	69.4	1—Failed in grip hole—		
1800	1800	0	75	T3CU-4	39.4	61.6	10.0	Base	0.45
		70	160	T3C4-3	45.7	68.3	10.0	Base	0.55
		140	240	T3C3-3	56.9	72.9	5.0	HAZ	0.15
		350	425	T3C1-3	60.2	75.1	6.0	Weld	0.10
		700	—No test —specimen fractured during machining—						
2200	2200	0	75	T3CU-3	35.2	48.9	15.0	Base	0.45
		70	150	T3C4-4	37.8	47.4	17.0	Base	0.30
		140	260	T3C3-4	39.6	50.3	16.0	Base	0.30
		350	420	T3C1-1	44.0	53.8	13.0	Base	0.30
		700	950	T3C2-4	48.7	56.0	7.0	Weld	0.07

(1) Heat affected zone
(2) Based on weight gain after diffusion anneal and as received oxygen content of 75 ppm.

TABLE 8. Tensile Test Properties of FS-85 at Five Oxygen Levels

Tensile Test Temp. (°F)	50-Hr. Diffusion Temp. (°F)	Contamination Level PPM O_2	Calculated (2) Total Oxygen Level	Specimen No.	Y. S. 0.2% Offset Psi x 10^3	Ultimate Stress Psi x 10^3	Elongation %	Fracture Location	Distance From Weld Centerline (inches)
		0	105	C3CU-1	64.3	84.5	20.0	Weld	0.04
		100	225	C3C5-1	58.7	86.7	23.0	Base	0.20
Room	1800	200	300	C3C2-3	60.8	87.7	21.0	Base	0.25
Temp.		500	600	C3C1-4	76.6	94.8	9.0	HAZ(1)	0.15
		1000	910	C3C4-1	80.3	96.1	6.0	Weld	0.05
		0	105	C3CU-3	31.4	52.1	16.0	Base	0.35
		100	195	C3C5-3	35.4	56.0	12.0	Weld	0.00
1500	1500	200	290	C3C2-1	41.1	57.7	9.0	HAZ(1)	0.12
		500	600	C3C1-1	47.2	60.0	5.0	Weld	0.00
		1000	890	C3C4-4	50.0	59.7	5.0	Weld	0.05
		0	105	C3CU-2	28.9	42.9	17.0	Base	0.37
		100	210	C3C5-2	30.8	45.1	16.0	Base	0.40
1800	1800	200	295	C3C2-2	33.3	45.9	16.0	Base	0.40
		500	640	C3C1-3	42.4	52.8	8.0	HAZ(1)	0.12
		1000	1090	C3C4-2	52.8	56.1	3.0	HAZ(1)	0.10
		0	105	C3CU-4	22.4	29.2	20.0	Weld	0.00
		100	200	C3C5-4	21.9	28.6	18.0	Weld	0.00
2200	2200	200	300	C3C2-4	22.0	28.8	25.0	Weld	0.00
		500	580	C3C1-2	23.7	29.3	27.0	Base	0.45
		1000	880	C3C4	No test				

(1) Heat affected zone
(2) Based on weight gain after diffusion anneal and as-received oxygen content of 105 ppm.

levels produce a change in the fracture location from the base metal to the weld and heat affected zone, Figures 30 and 34. Presumably, some of the oxygen strengthening is lost in the weld and heat affected zone. As at 1500°F, the fracture appearance of FS-85 is ductile at all oxygen levels, Figure 38. No complete comparison is provided for T-111 and T-222 since the high oxygen level specimens fractured during machining or through the pin grip hole during testing, indicating extremely low ductility.

Room Temperature Tensile Specimens

These specimens, sharing a common thermal history with the 1800°F tensile specimens (diffusion annealed at the same temperature) display the same shift in fracture location, from the base metal to weld area, with increasing oxygen content, Figures 31, 35, and 39. The room temperature test conditions result in high yield and tensile strengths, but the tensile elongation values are comparable to the 1500°F and 1800°F test temperatures, Figures 22, 25 and 28. This is apparently the result of increased strain hardening preventing localized yielding and necking. The fracture appearance is not as ductile as at 1800°F with several microcracks observable in the lowest oxygen level FS-85 sample, Figure 39. Referring to the same figure, increasing oxygen content does not reduce the ductility of the fracture although the overall tensile elongation data, Figure 28, shows a moderate decrease to 6% elongation for the highest oxygen level. The high oxygen level fracture for T-111, Figure 31, shows the fracture through a zone of heavy precipitation which was over etched during metallographic preparation. This will be further explored in the second phase of this program which is a more thorough study of T-111.

2200°F Tensile Specimens

At this temperature the oxygen reactions no longer result in as significant strengthening, possibly because of reactions broadly classified as overaging, such as the coalescence of finely divided and coherent oxides or the formation of different complex oxides. A limited amount of metallographic work will be done in an attempt to correlate the observed structure with physical property changes and provide a rationale for the effect of oxygen

contamination. Fracture appearance is ductile with some tendency for grain boundary sliding in the higher oxygen content tantalum base alloys, Figures 32 and 36. Overall tensile elongation is high with the oxygen contaminated FS-85 showing better elongation than uncontaminated material, Figure 28. The fracture appearance, Figure 40, indicates that oxygen may be preventing massive grain growth and subsequent grain boundary separation which is characteristic of FS-85[9] at 2200°F. Weld cross sections of the five oxygen levels will be evaluated for the effect of oxygen on weld and heat affected zone grain size.

Specific Alloy Response to Oxygen Contamination

T-111 - Increasing oxygen contamination produces a uniform increase in yield and tensile strength. Tensile elongation is similarly reduced with oxygen content. The highest oxygen level, 700 wt ppm oxygen, reduced ductility to such an extent that the 1800°F tensile test specimen failed through the pin grip hole. Fracture appearance, Figures 29 through 32, was ductile at all but the highest oxygen level. At the highest oxygen level, intergranular fracture became the predominant mode, including grain boundary sliding at 2200°F. The fracture location was consistently in the base metal in the uncontaminated condition. Increasing oxygen content was associated with fractures in the weld and heat affected zone in specimens diffusion annealed at 1800°F (room temperature and 1800°F specimens). However, at 1500°F and 2200°F, the fractures remained predominantly in the base metal. As a check on the overall program results, the baseline data obtained from uncontaminated specimens is similar to existing[9] tensile test data. A significant difference is noted in fracture location which lies in the base metal for this study and consistently in the weld for the comparative samples. The explanation may lie in the anisotropic tensile properties of T-111[11]. This alloy is weaker parallel to the rolling direction which is the orientation of the tensile specimens in this study. Previously reported data is of weld specimens with the tensile specimen axis transverse to the rolling direction.

T-222 - Similar behavior to T-111 was observed with respect to response to oxygen contamination. An even more marked increase in yield strength, Figure 23, was observed

at 1800°F with increasing oxygen content. The loss in ductility, as measured by tensile elongation, was more severe in T-222 than T-111, Figures 22 and 25. Perhaps an even better measure of the engineering properties of the metal was provided by material handling problems with the tensile specimens. Of the four high oxygen level samples, two were fractured during machining and one failed through the pin grip hole during loading. In view of the painstaking care employed in machining (electro-discharge machining and grinding was used), this indicates extreme room temperature brittleness. Fracture location with respect to temperature and oxygen content was similar to T-111, all uncontaminated specimens fracturing in the base metal. The specimens diffusion annealed at 1800°F (room temperature and 1800°F tensile specimens), show a definite fracture location shift to the weld and heat affected zone with increasing oxygen content. The 1500°F and 2200°F specimens predominantly fracture in the base metal at all oxygen levels. The tensile properties of the uncontaminated specimens are comparable to previously reported data [9] on transverse weld specimens. As with T-111, however, the fracture location is in the base metal rather than in the weld and heat affected zone. The effect of specimen orientation, as mentioned in the T-111 section, is believed to be the reason. Fracture appearance, Figures 33 through 36, is ductile at all oxygen levels although only one valid specimen was obtained for the 700 ppm oxygen level, the other three specimens either fractured prematurely during preparation or failed in the pin grip instead of the gage length.

FS-85 - The effect of oxygen additions on tensile behavior is similar to the tantalum base alloys with the exception that the strengthening effects are more marked at 1500°F and are completely lost at 2200°F. Basically, tensile and yield strength is increased and elongation is decreased with oxygen additions. The fracture location does not show the clear cut dependence on oxygen level as noted in the tantalum base alloys. The 1500°F and 1800°F specimens do show a shift from the base metal to the weld and heat affected zone with increasing oxygen content, but the room temperature specimens, diffusion annealed at 1800°F, show a mixed response, Figure 39. The 2200°F, uncontaminated specimen, Figure 40, shows a massive, intergranular fracture surface typical of FS-85 at this temperature range. The higher oxygen level specimen (500 ppm O_2), fractured in the

base metal with high total elongation, but low visible straining in the weld area. All fracture surfaces are ductile in appearance, up to the highest oxygen levels. The data for the uncontaminated specimens may be compared, with some qualifications because of specimen orientation and thermal history, to previously reported transverse weld data[10] for FS-85. The comparison shows significantly higher yield strength and improved elongation at 1800°F and 2200°F for the specimens in this study phase. Since there was also a difference in fracture location, half of the present specimens fractured in the base metal versus none for the previously reported data, it is assumed that the welds in this phase are stronger. It is suspected that the 2400°F - 1 hour post weld annealing treatment unique to the previously reported data is responsible for the lower weld strength. The tensile properties of FS-85 were not markedly degraded by oxygen contamination up to 1000 ppm. All contaminated specimen fractures had a ductile appearance and at the highest temperature fracture behavior was actually improved by oxygen additions.

The moderate difference between T-111 and T-222 in tensile strength response to oxygen contamination may be explained in terms of solute and as-received interstitial content differences. The measured difference in composition is shown below:

	Hafnium	Tungsten	Carbon	Oxygen	Nitrogen	Total Interstitial
T-111	2.0%	8.8%	35 ppm	40 ppm	25 ppm	100 ppm
T-222	2.6%	9.2%	110 ppm	75 ppm	5 ppm	190 ppm

The previously reported[9] marked difference in bend ductility, however, is not so easily explained. A possibility being presently investigated is that the 25% higher hafnium content has a marked effect on the diffusion rate of oxygen into the matrix. A severe oxygen gradient would produce a brittle surface layer which would greatly influence the bend ductility performance.

IV. FUTURE WORK

Bend ductility tests of both the welds and base metal will be completed for the second phase

of the oxygen contaminated weldability program along with a more detailed evaluation of T-111 which includes the effect of 1000-hour aging at 1500°F, 1800°F, and 2200°F on oxygen contaminated material. Tensile tests at ambient and elevated temperatures will be completed on aged specimens. Metallographic examinations will be continued, including phase identification and microhardness traverses to correlate the microstructure with the observed changes in physical properties as influenced by oxygen level and thermal history. Chemical analyses will be obtained for oxidized samples with successive layers machined from the surface as supporting evidence for microhardness traverses in following the diffusion of oxygen through the material thickness.

Additional data will become available on the thermal stability evaluation of refractory metal alloys in general. This will include data on ten alloys which have been aged through 1000 hours at temperatures between 1500°F and 2400°F. All alloys were "in process" during this period so that a discussion of this effort was omitted from this report.

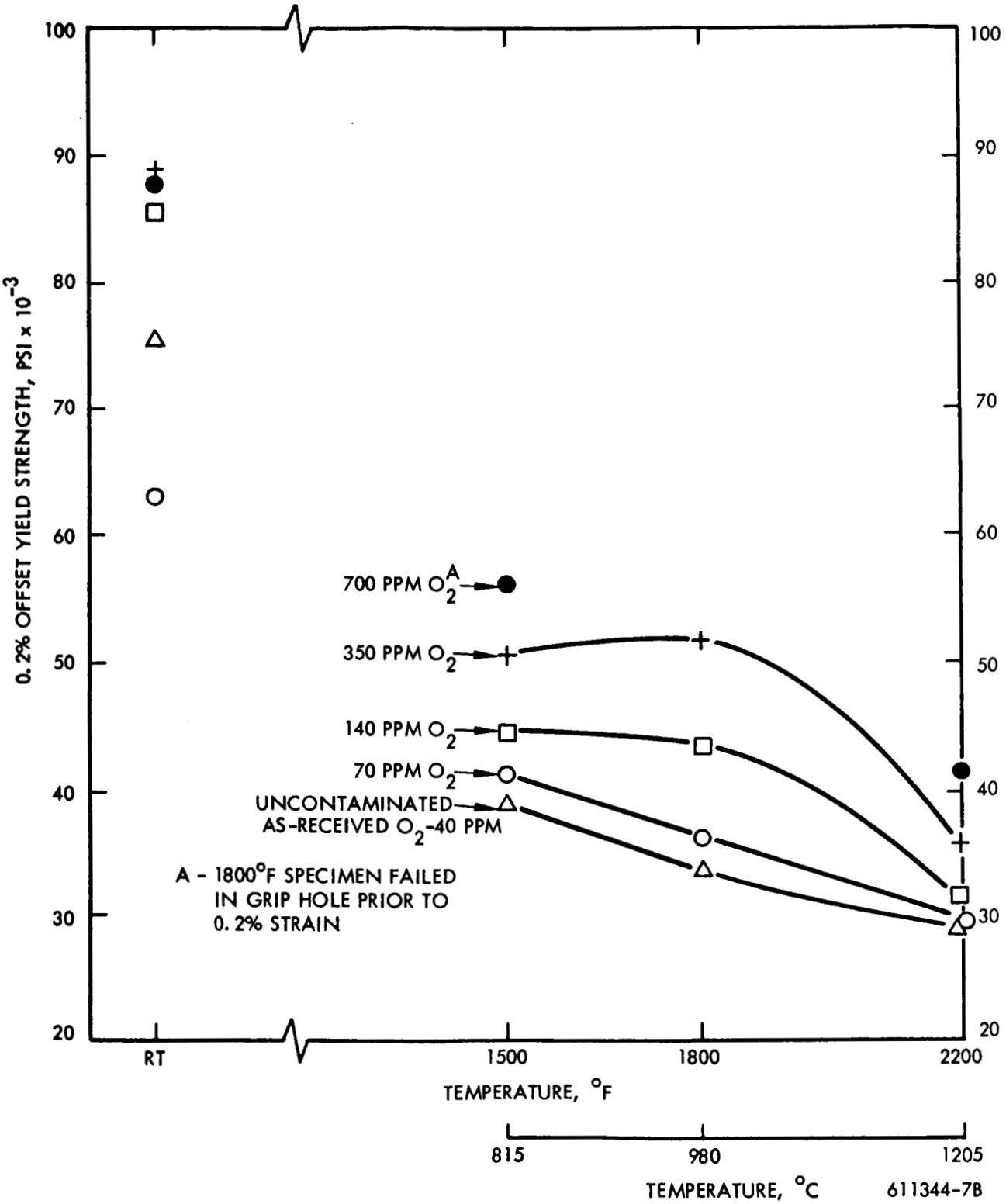


FIGURE 20 - T-111, Yield Strength Versus Temperature at 5 Oxygen Levels

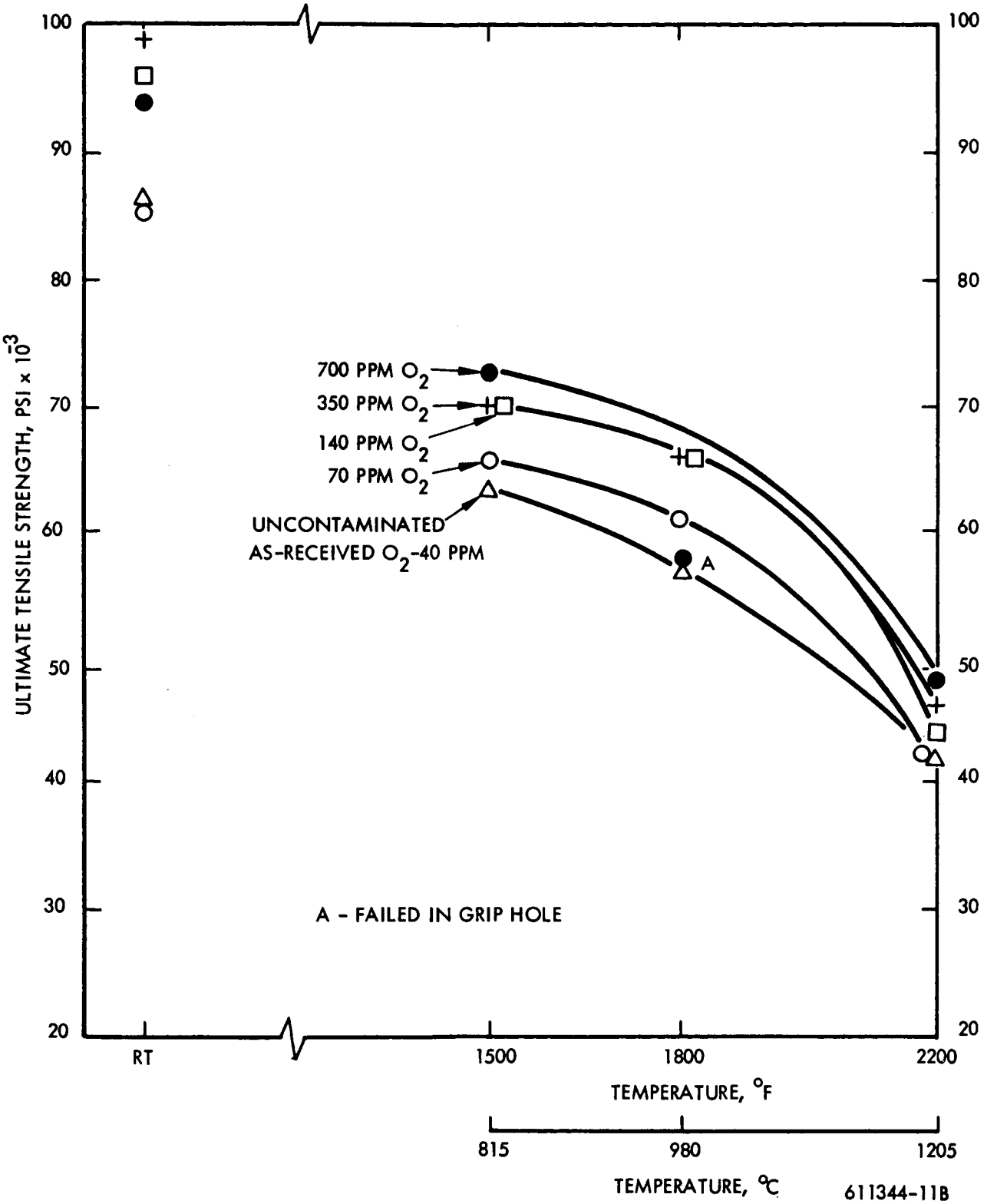


FIGURE 21 - T-111, Tensile Strength Versus Temperature at 5 Oxygen Levels

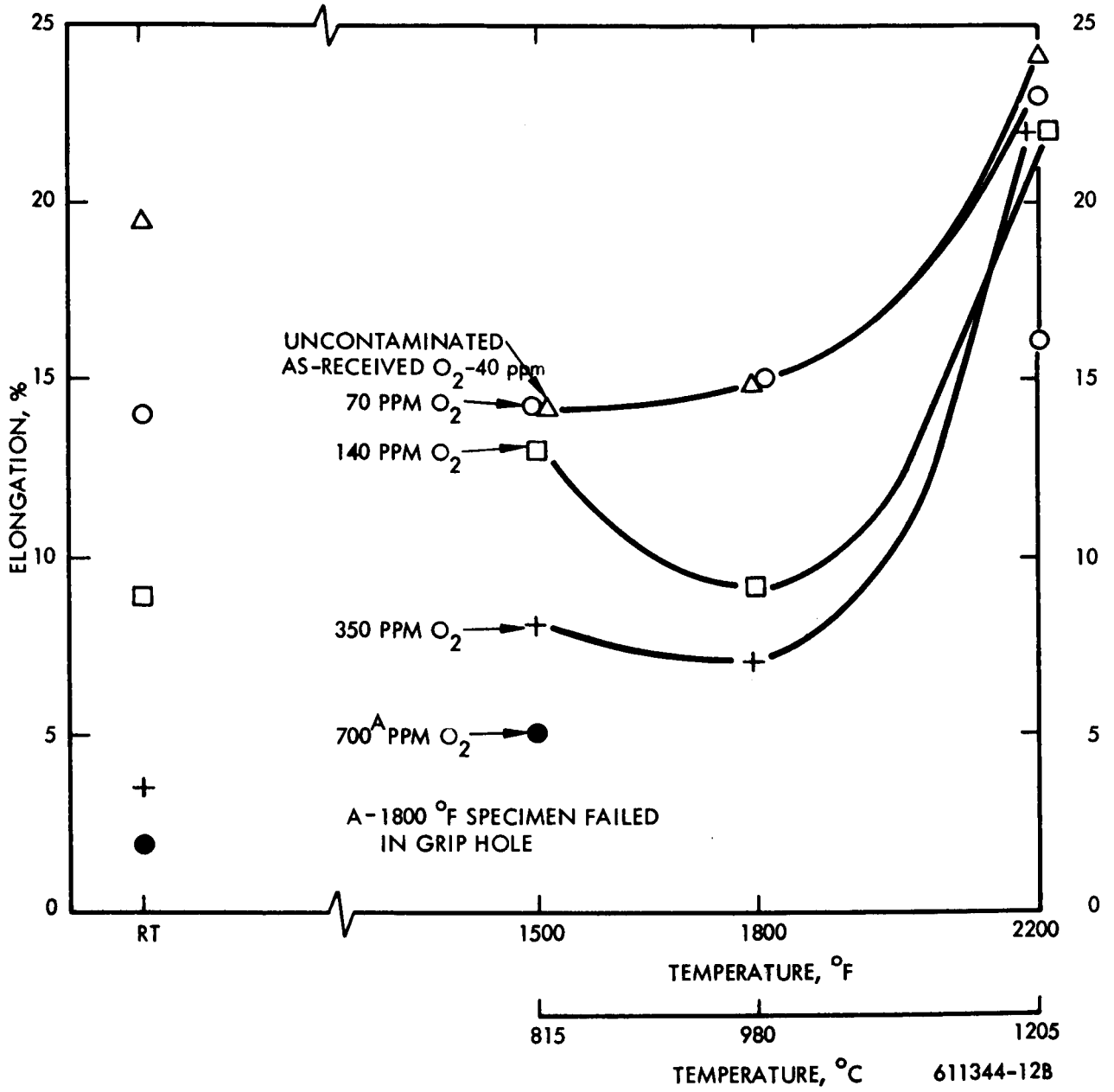


FIGURE 22 - T-111, Elongation Versus Temperature at 5 Oxygen Levels

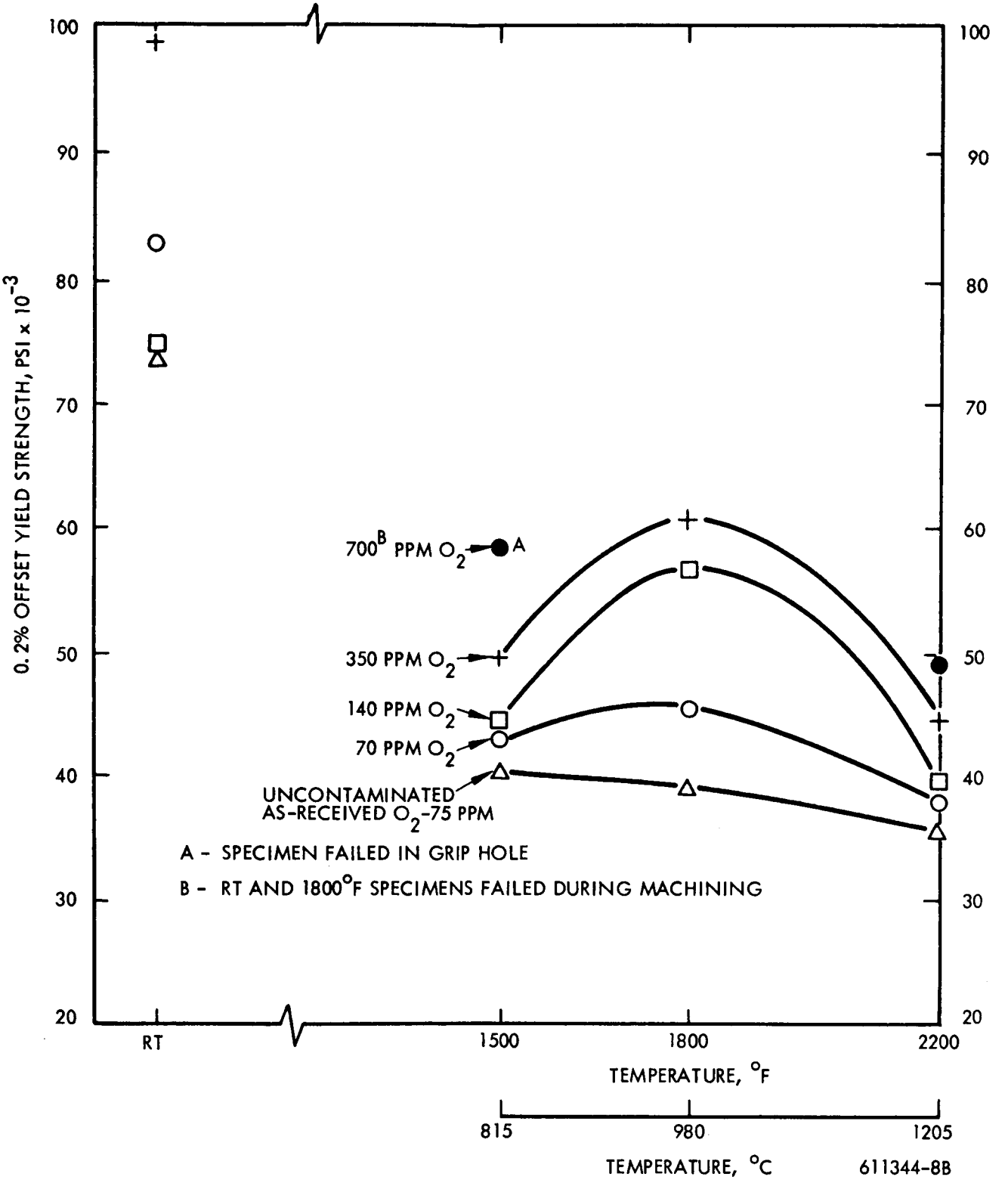


FIGURE 23 - T-222, Yield Strength Versus Temperature at 5 Oxygen Levels

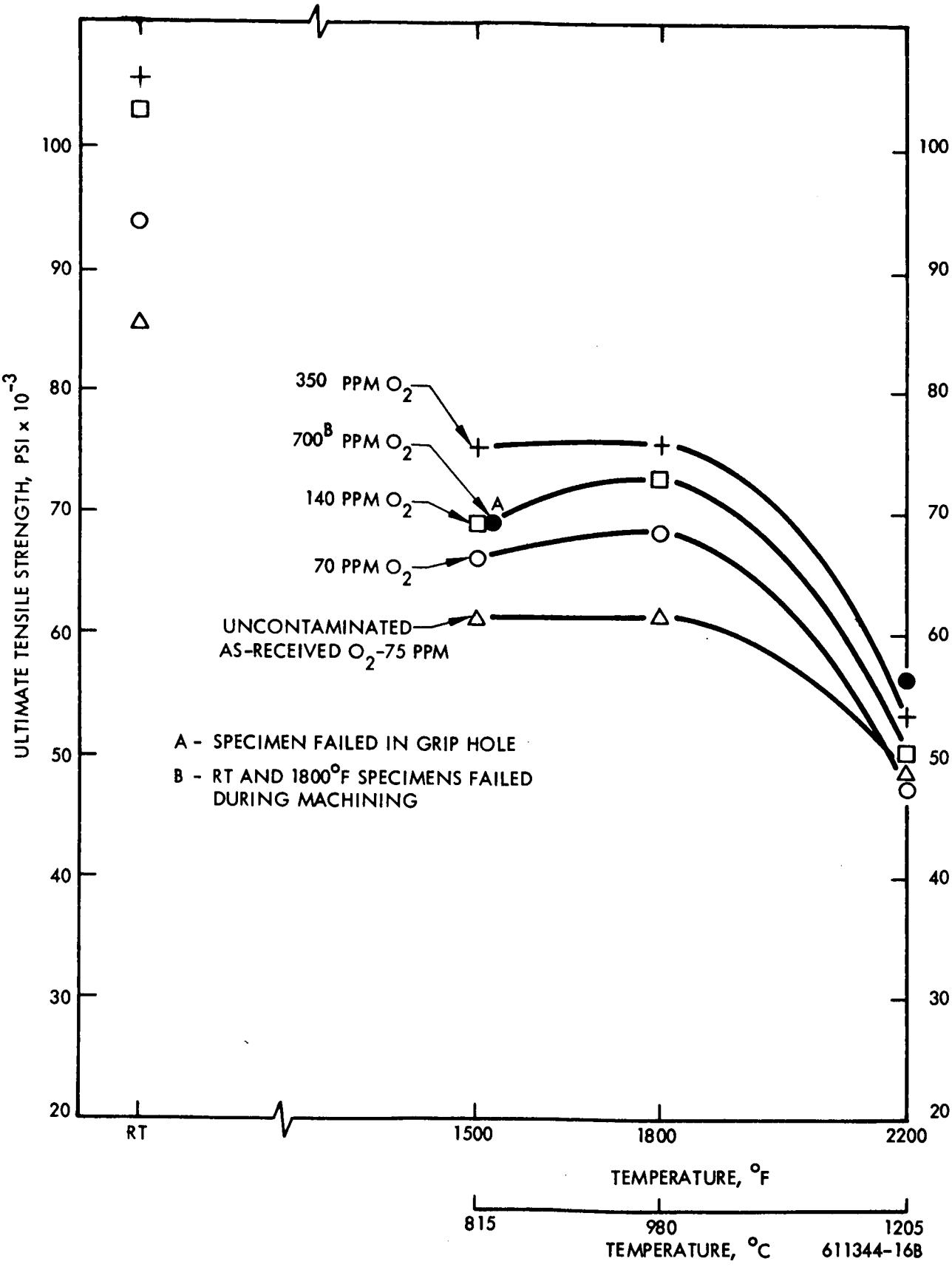


FIGURE 24 - T-222, Tensile Strength Versus Temperature at 5 Oxygen Levels

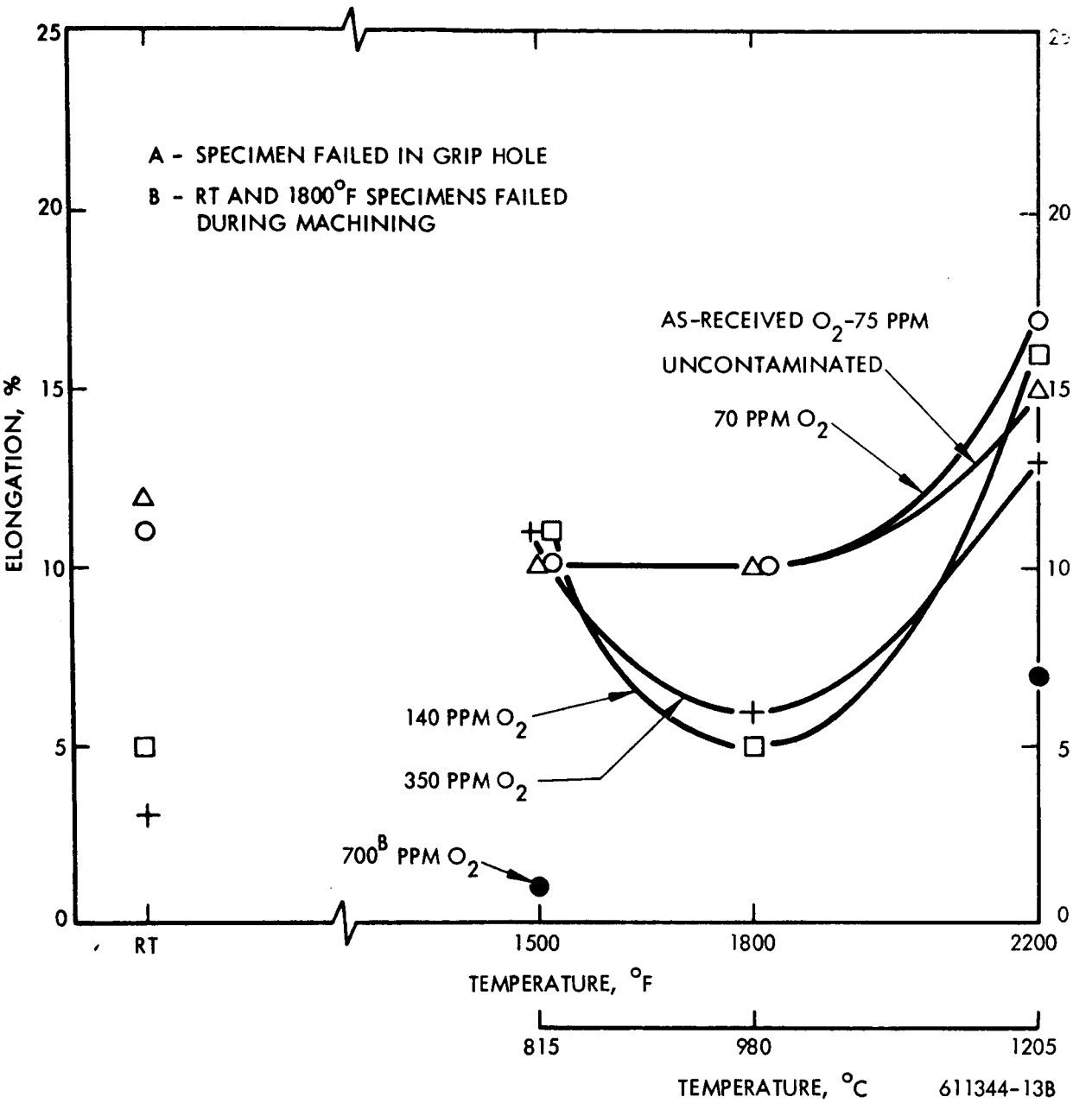


FIGURE 25 - T-222, Elongation Versus Temperature at 5 Oxygen Levels

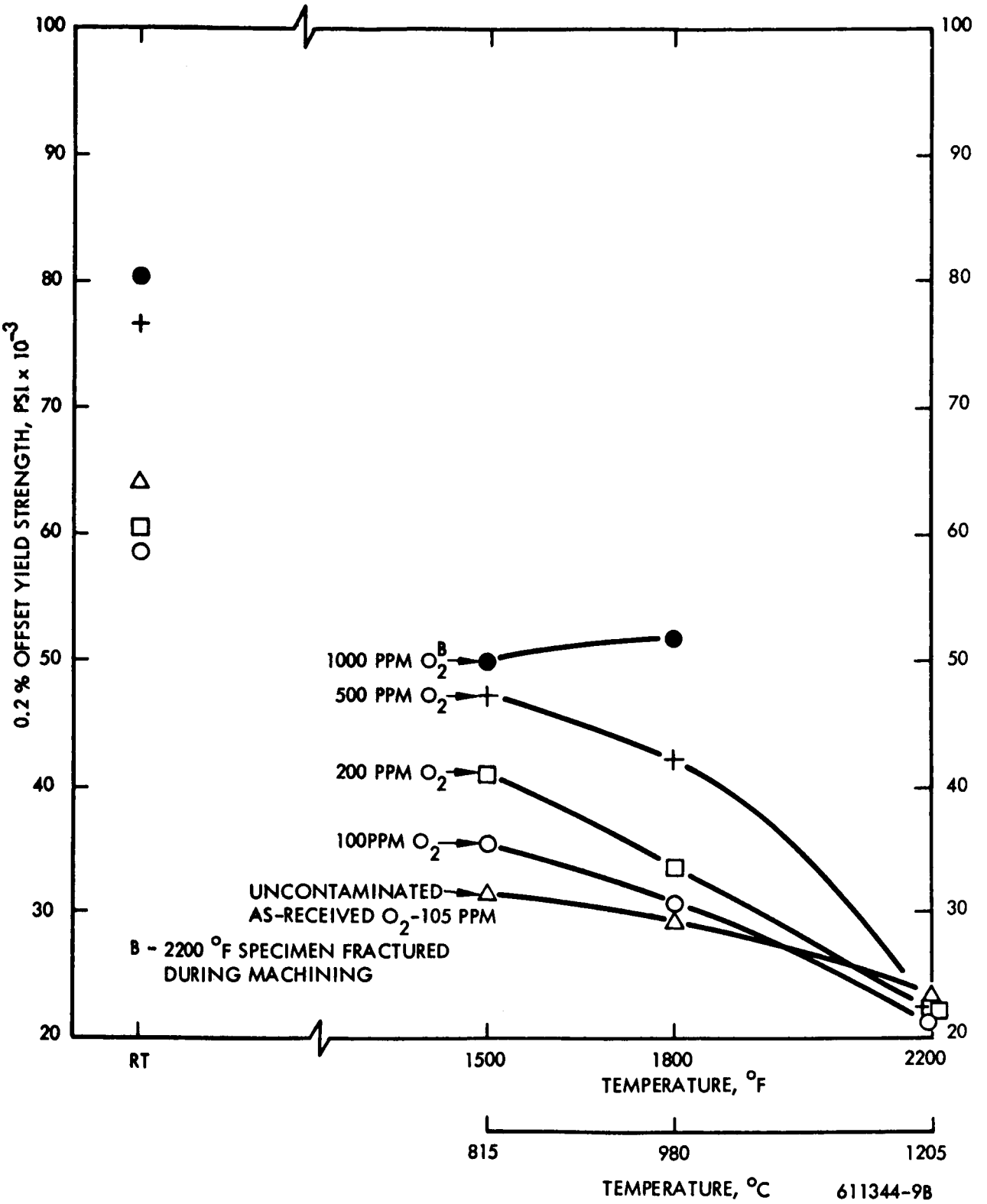


FIGURE 26 - FS-85, Yield Strength Versus Temperature at 5 Oxygen Levels

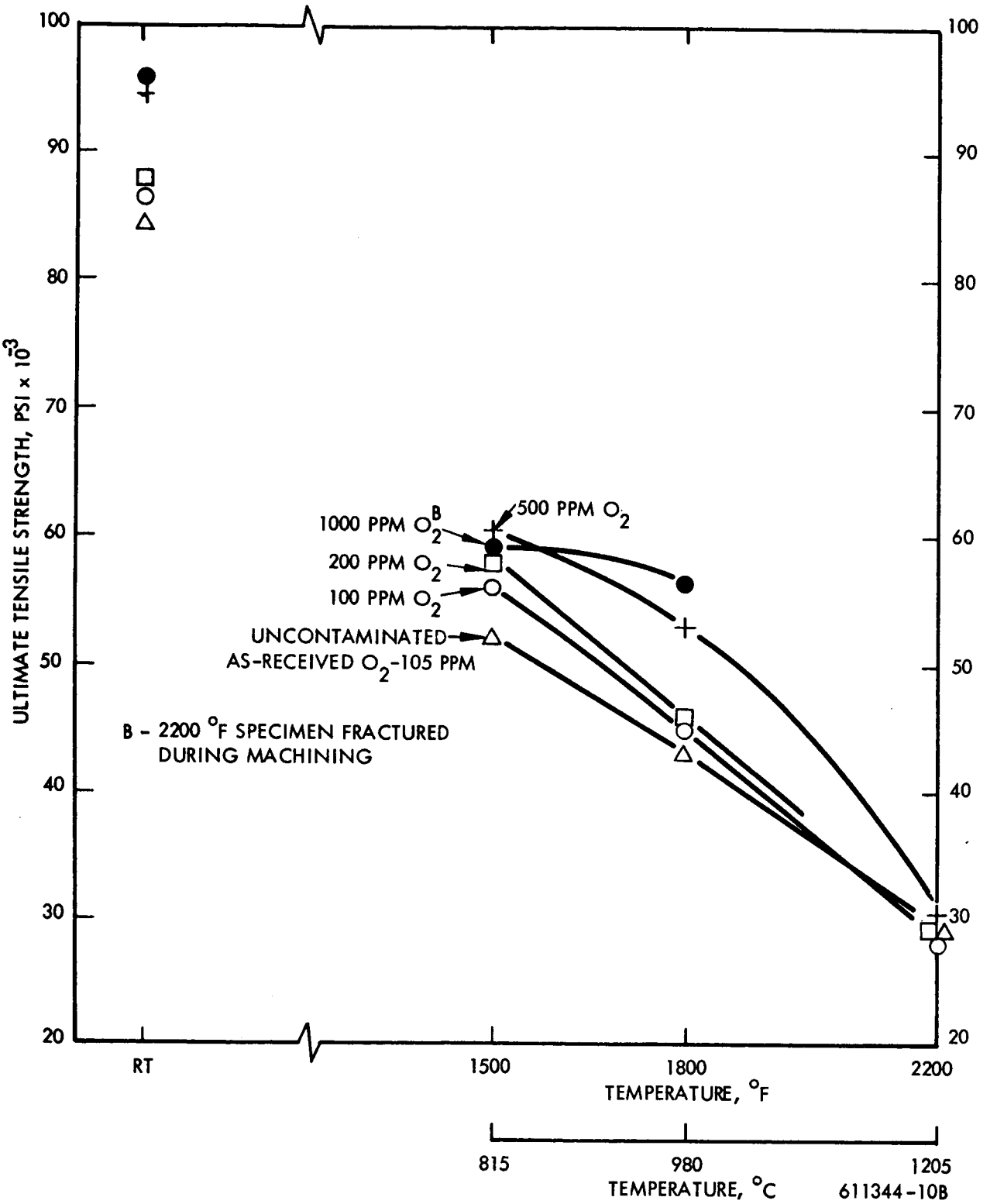


FIGURE 27 - FS-85, Tensile Strength Versus Temperature at 5 Oxygen Levels

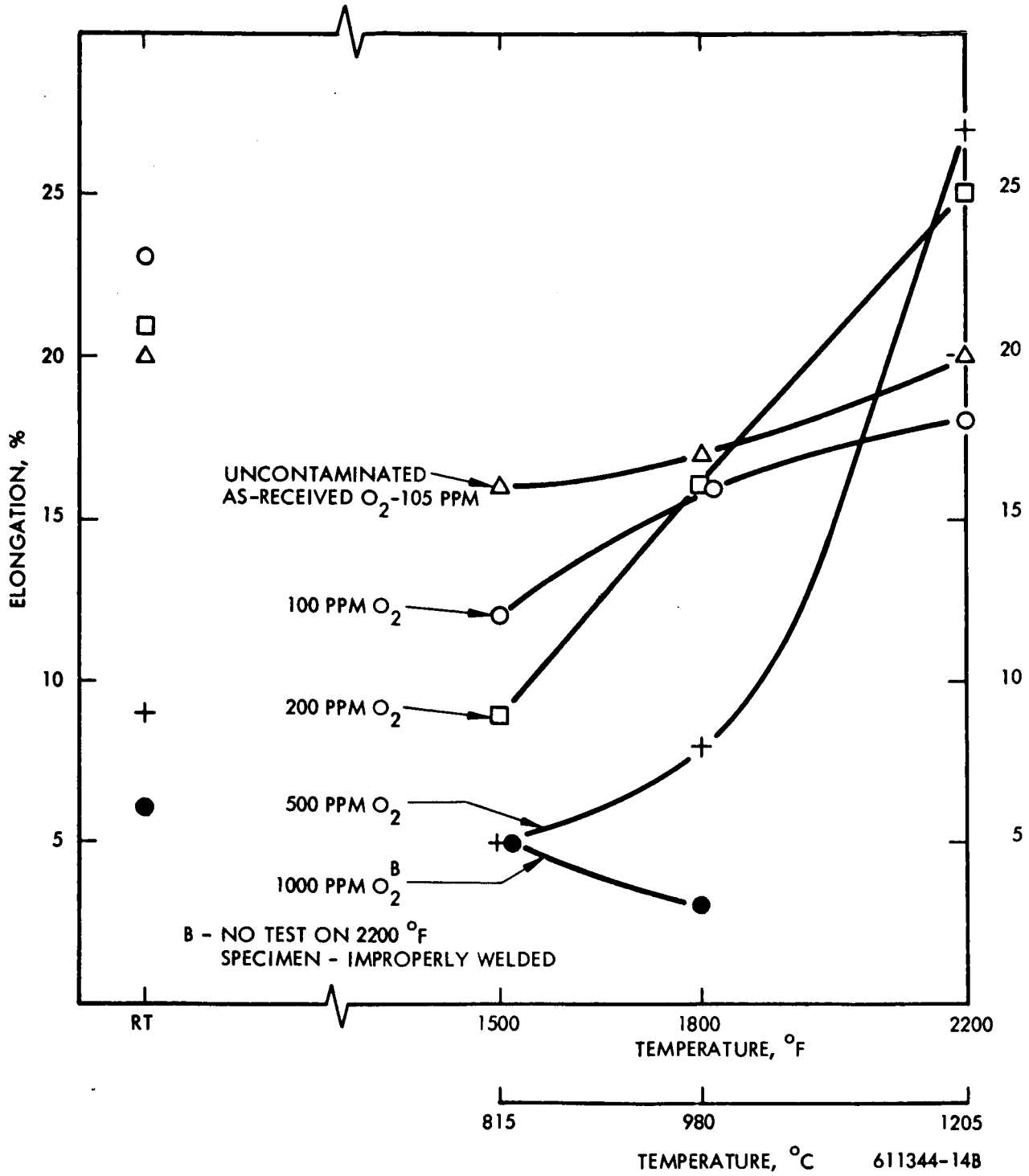
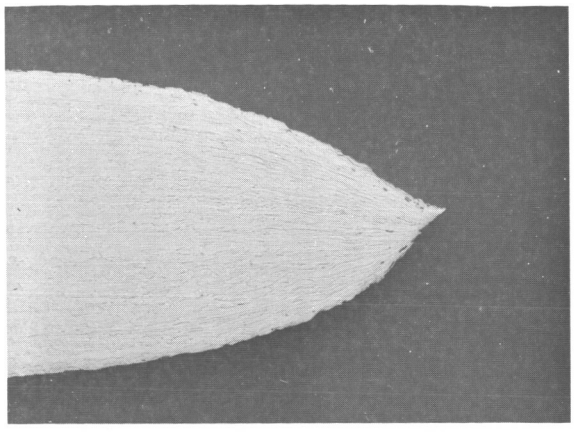
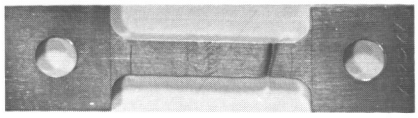


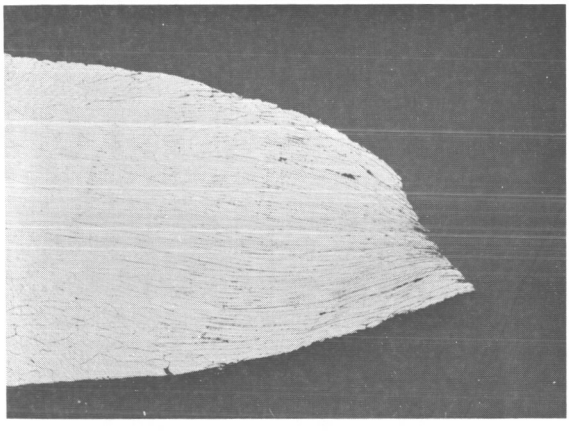
FIGURE 28 - FS-85, Elongation Versus Temperature at 5 Oxygen Levels



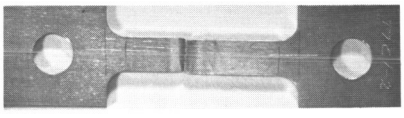
12,157 60X



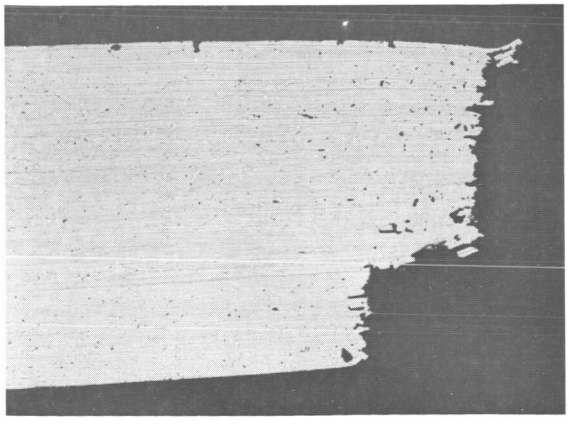
TICU-1
Base Metal Fracture
Uncontaminated
40 ppm Oxygen



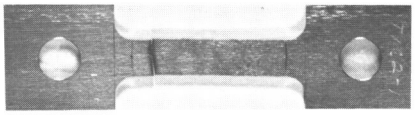
12,158 60X



TICI-2
Weld Fracture
380 ppm Oxygen

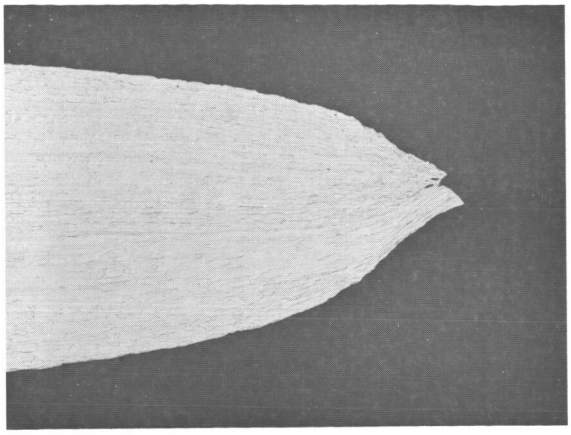


13,576 60X

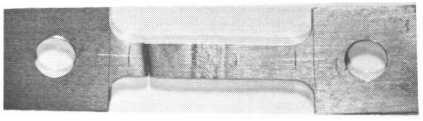


TIC2-1
Base Metal Fracture
810 ppm Oxygen

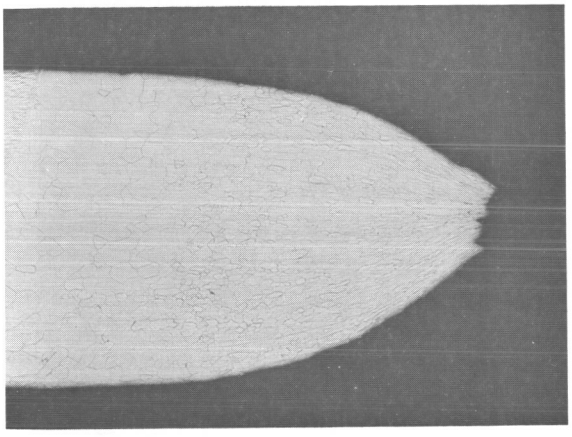
FIGURE 29 - T-111, Photographs of 1500°F Tensile Specimens



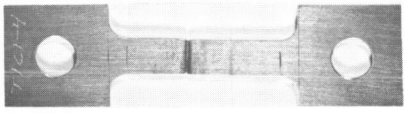
12,163 60X



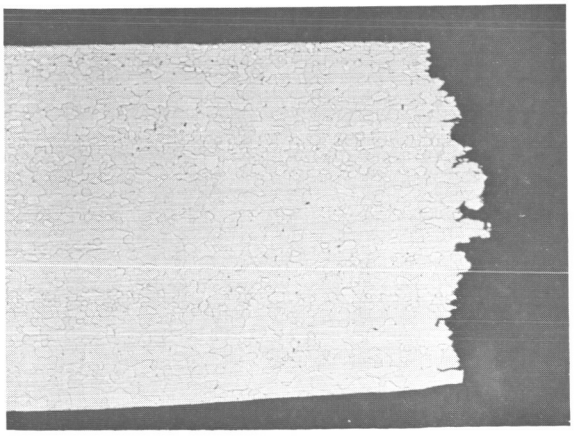
TICU-4
Base Metal Fracture
Uncontaminated
40 ppm Oxygen



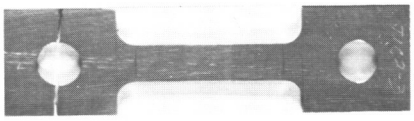
12,164 60X



TICI-4
Heat Affected Zone Fracture
370 ppm Oxygen

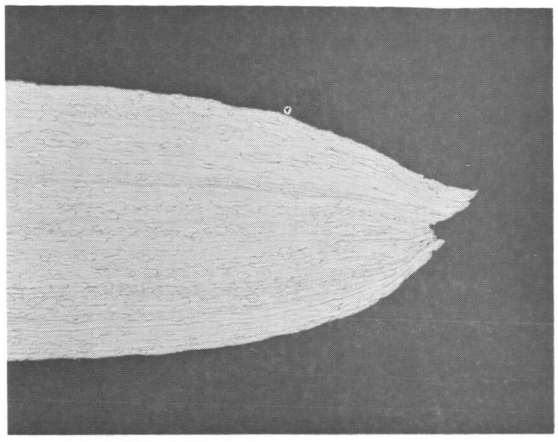


13,577 60X

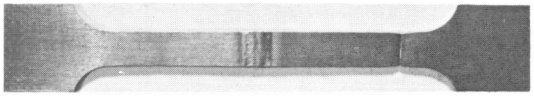


Grip Hole Failure
810 ppm Oxygen

FIGURE 30 - T-111, Photographs of 1800°F Tensile Specimens



12,151 60X

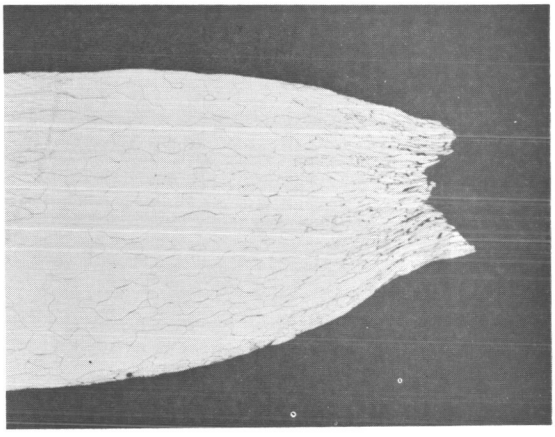


TICU-3

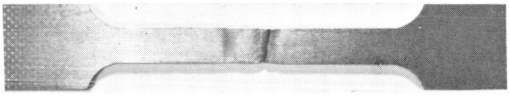
Base Metal Fracture

Uncontaminated

40 ppm Oxygen



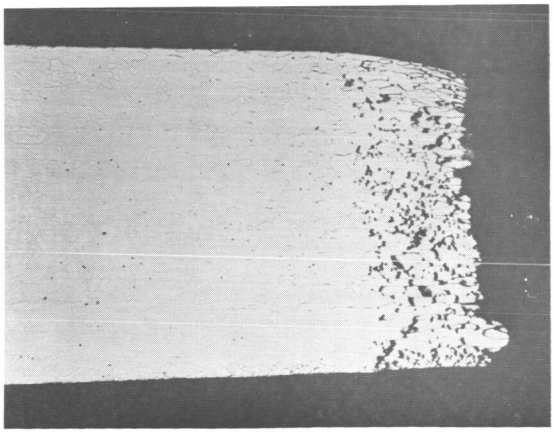
12,152 60X



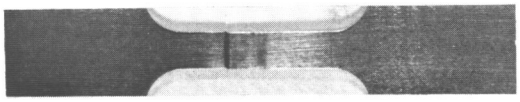
TICI-3

Heat Affected Zone Fracture

360 ppm Oxygen



13,575 60X

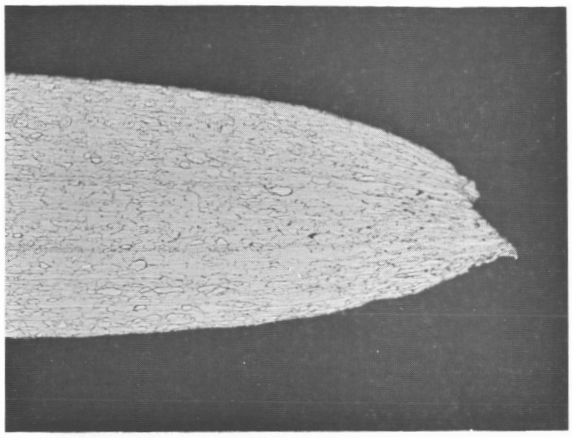


TIC2-2

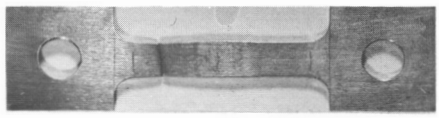
Heat Affected Zone Fracture

800 ppm Oxygen

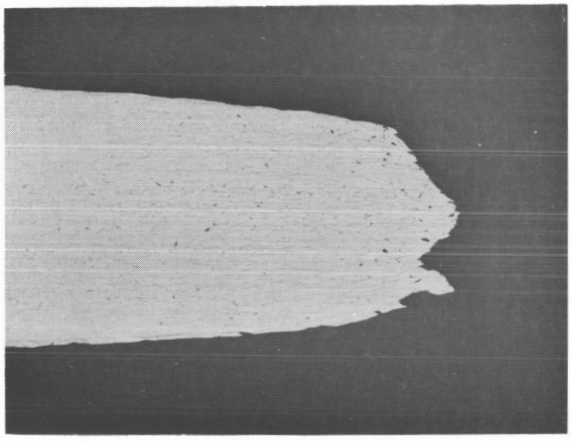
FIGURE 31 - T-111, Photographs of Room Temperature Tensile Specimens



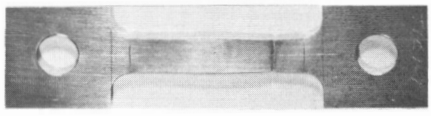
13,885 60X



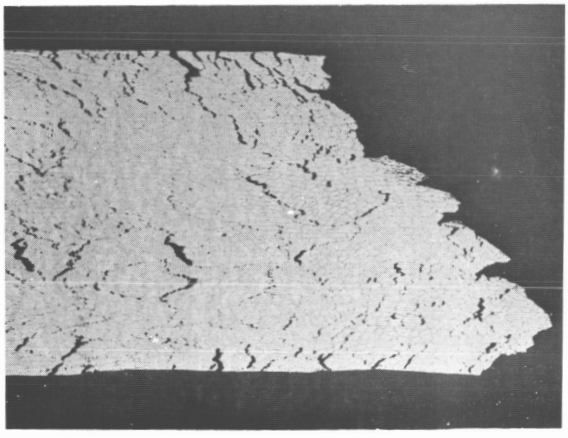
TICU-2
Base Metal Fracture
Uncontaminated
40 ppm Oxygen



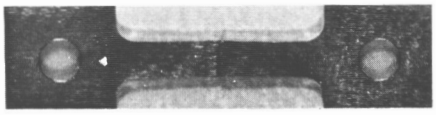
12,170 60X



TICI-1
Base Metal Fracture
380 ppm Oxygen

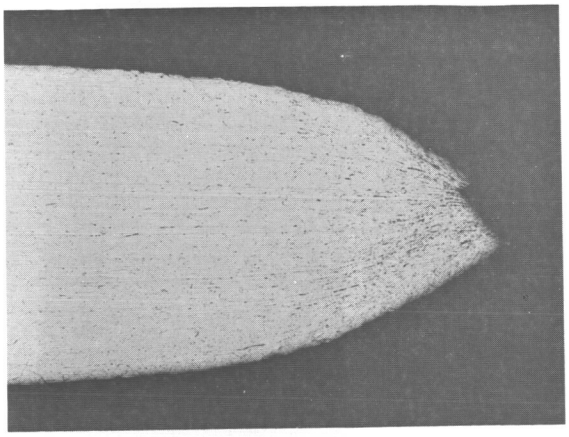


13,578 60X

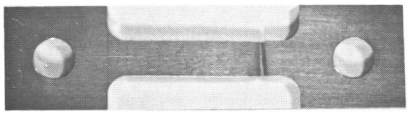


TIC2-4
Weld Metal Fracture
810 ppm Oxygen

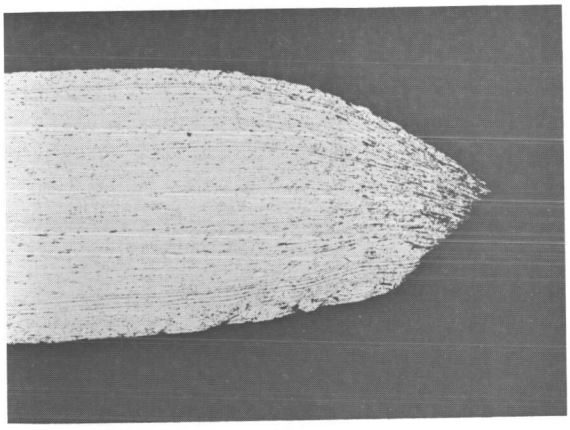
FIGURE 32 - T-111, Photographs of 2200°F Tensile Specimens



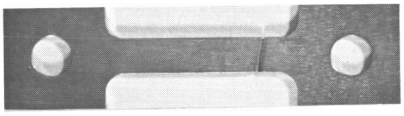
12,159 60X



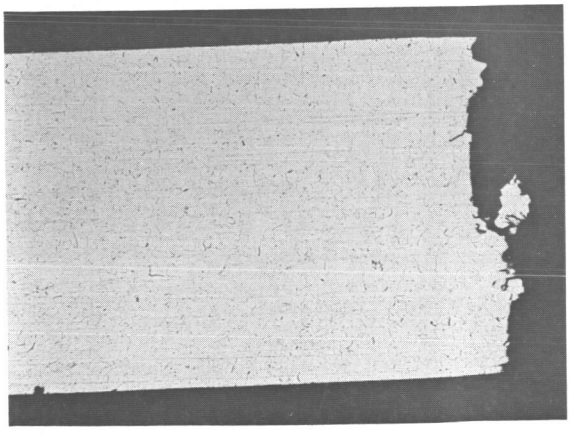
T3CU-1
Base Metal Fracture
Uncontaminated
75 ppm Oxygen



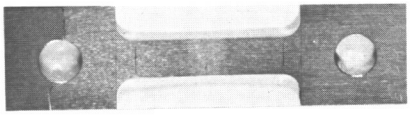
12,160 60X



T3CI-4
Base Metal Fracture
370 ppm Oxygen

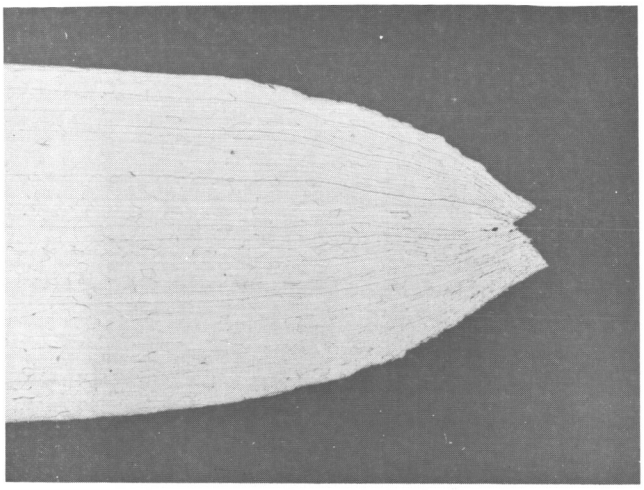


13,579 60X



T3C2-3
Grip Fracture
950 ppm Oxygen

FIGURE 33 - T-222, Photographs of 1500°F Tensile Specimens

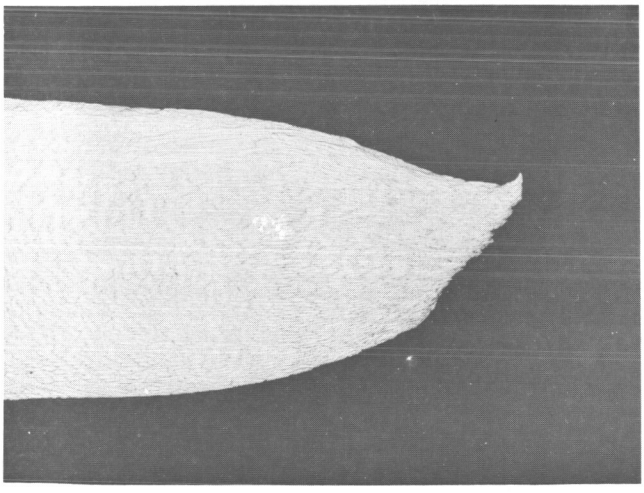


12,165 60X

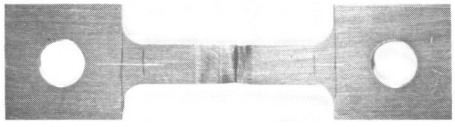


T3CU-4

Base Metal Fracture
Uncontaminated
75 ppm Oxygen



12,166 60X

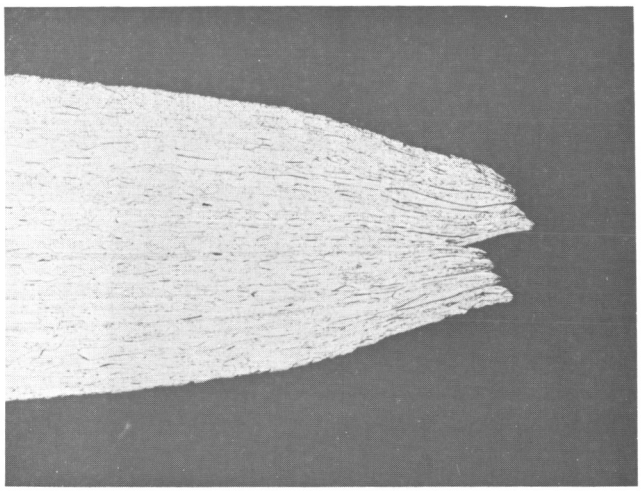


T3CI-3

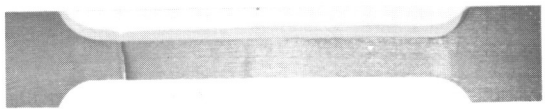
Weld Fracture
425 ppm Oxygen

No Test Specimen
Fractured During Machining

FIGURE 34 - T-222, Photographs of 1800°F Tensile Specimens



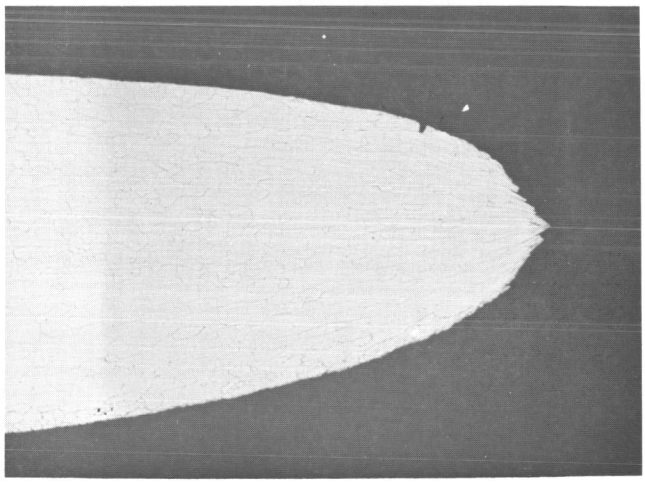
12,153 60X



T3CU-2

Base Metal Fracture

Uncontaminated
75 ppm Oxygen



12,154 60X



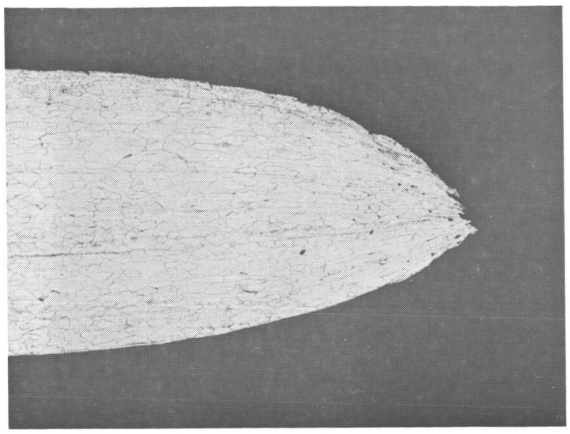
T3CI-2

Heat Affected Zone Fracture

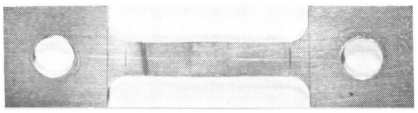
360 ppm Oxygen

No Test
Specimen Fractured During
Machining

FIGURE 35 - T-222, Photographs of Room Temperature Tensile Specimens



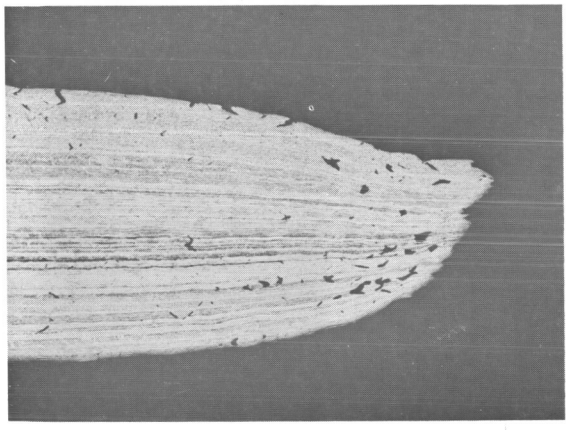
12,171 60X



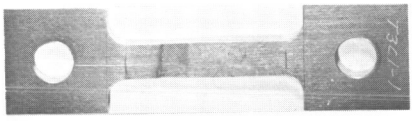
T3CU-3

Base Metal Fracture

Uncontaminated
75 ppm Oxygen



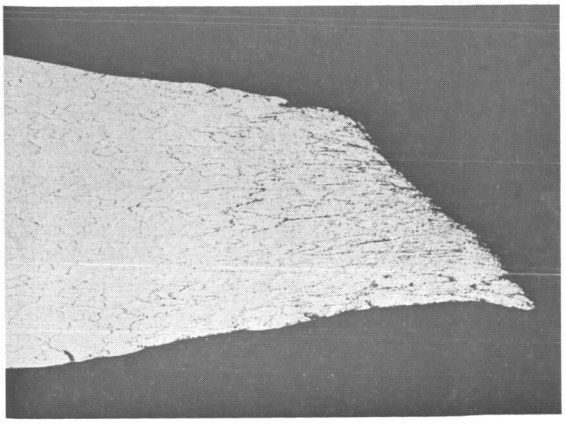
12,172 60X



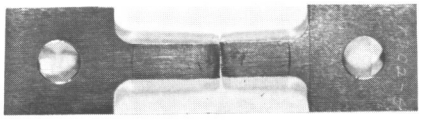
T3CI-1

Base Metal Fracture

420 ppm Oxygen



13,580 60X

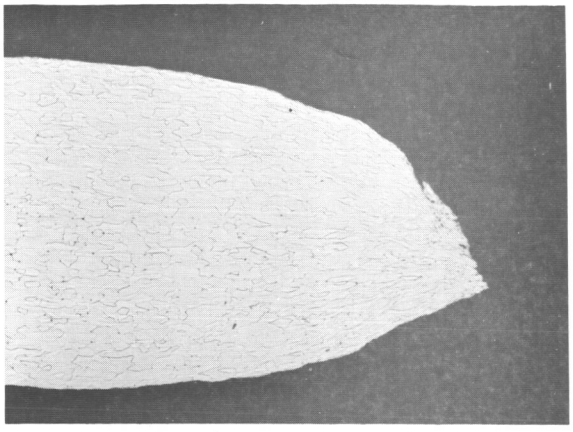


T3C2-4

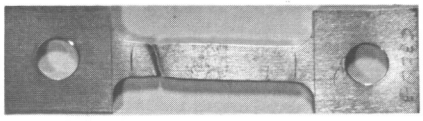
Weld Metal Fracture

950 ppm Oxygen

FIGURE 36 - T-222, Photographs of 2200°F Tensile Specimens



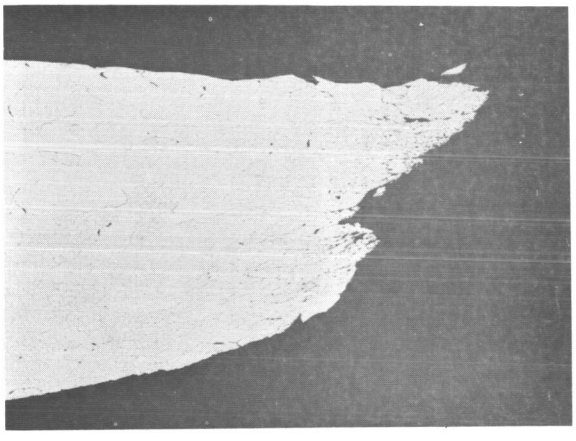
12,155 60X



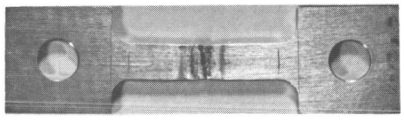
C3CU-3

Base Metal Fracture

Uncontaminated
105 ppm Oxygen



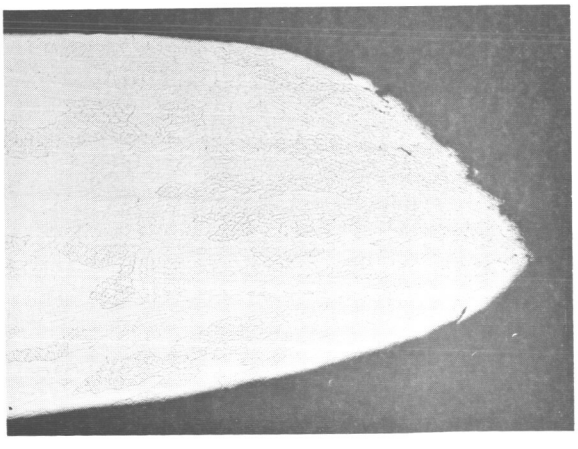
12,156 60X



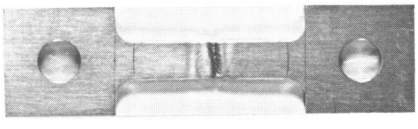
C3CI-1

Weld Metal Fracture

600 ppm Oxygen



13,573 60X

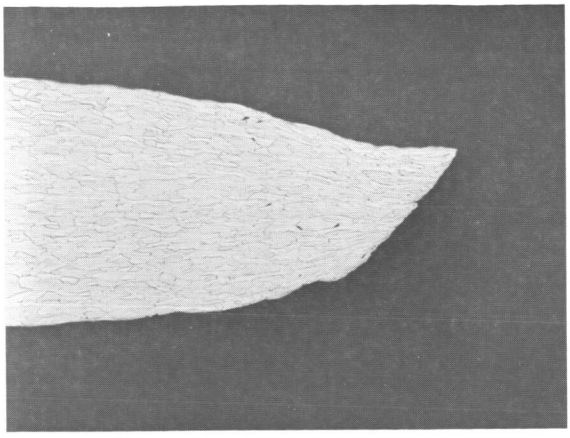


C3C4-4

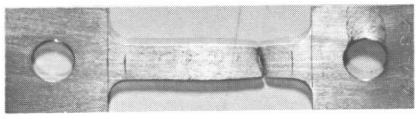
Weld Metal Fracture

890 ppm Oxygen

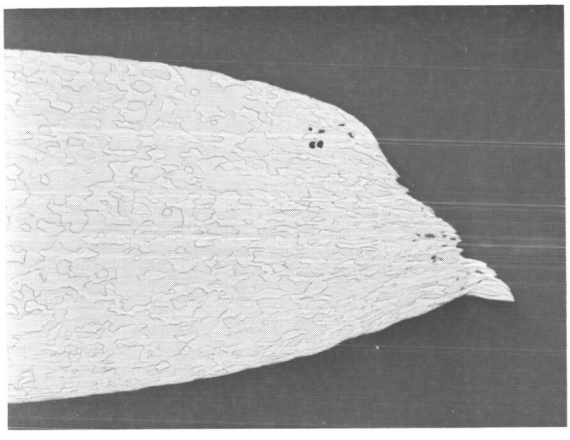
FIGURE 37 - FS-85, Photographs of 1500°F Tensile Specimens



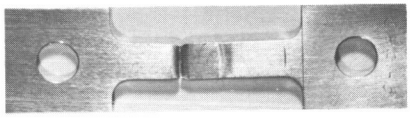
12,161 60X



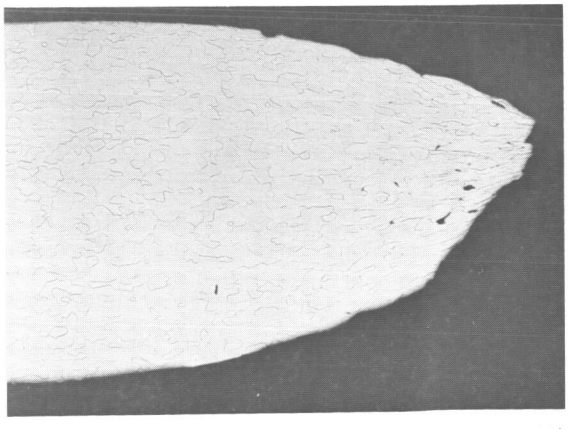
C3CU-2
Base Metal Fracture
Uncontaminated
105 ppm Oxygen



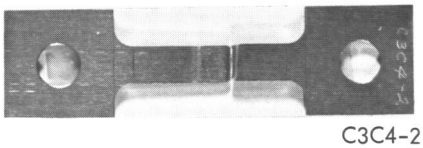
12,162 60X



C3CI-3
Heat Affected Zone Fracture
640 ppm Oxygen

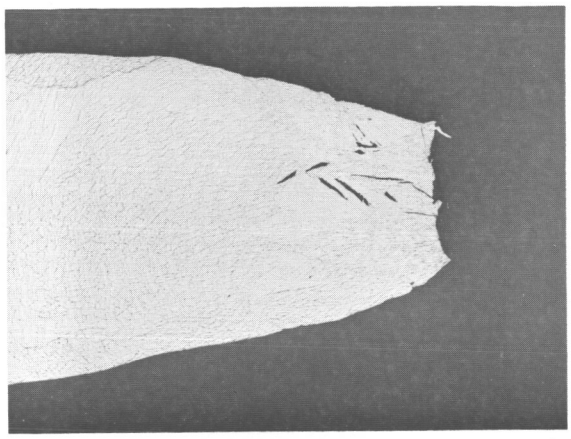


13,574 60X

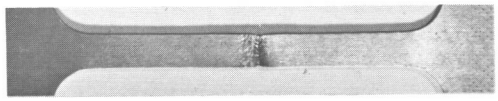


C3C4-2
Heat Affected Zone Fracture
1090 ppm Oxygen

FIGURE 38 - FS-85, Photographs of 1800°F Tensile Specimens



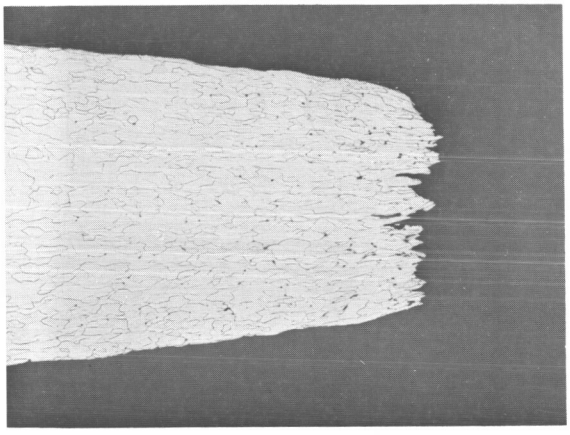
12,149 60X



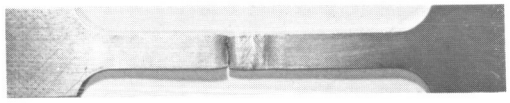
C3CU-1

Weld Fracture

Uncontaminated
105 ppm Oxygen



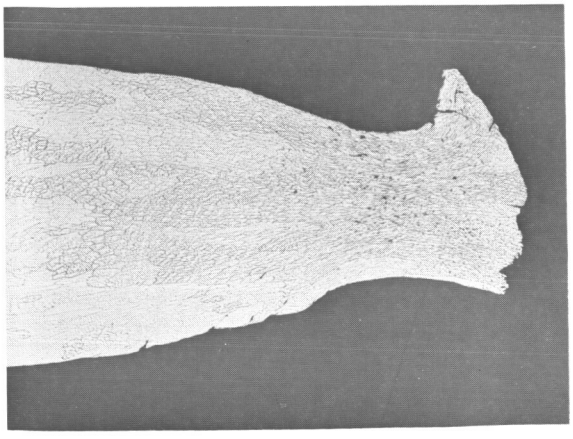
12,150 60X



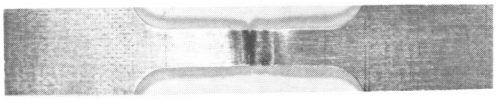
C3CI-4

Heat Affected Zone Fracture

600 ppm Oxygen



13,572 60X

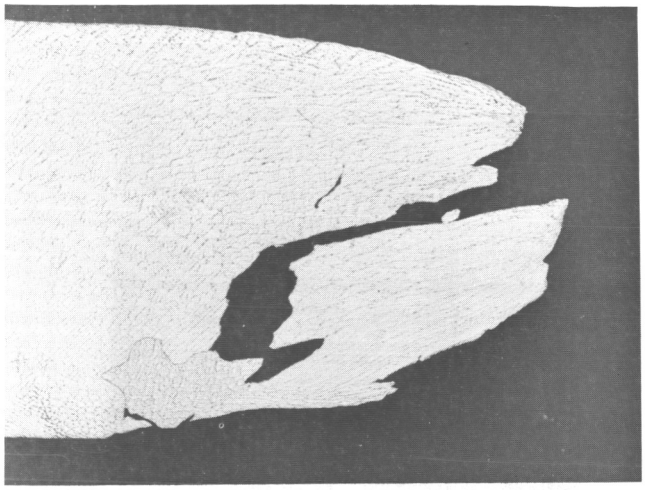


C3C4-1

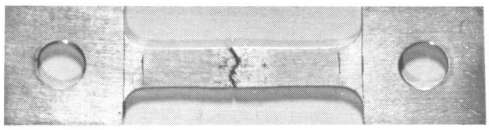
Weld Fracture

910 ppm Oxygen

FIGURE 39 - FS-85, Photographs of Room Temperature Tensile Specimens



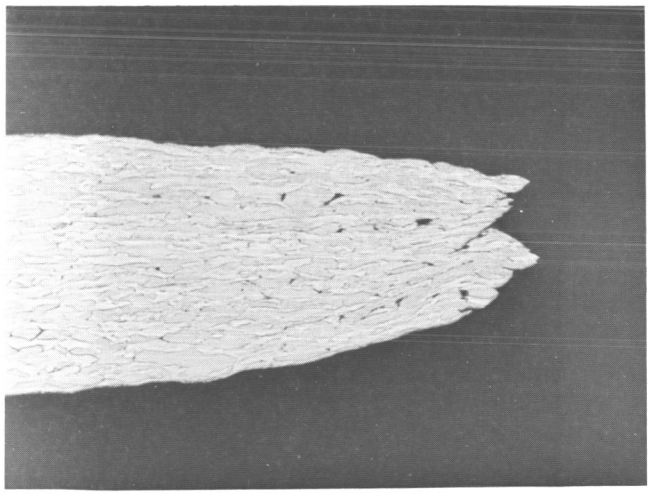
12,167 60X



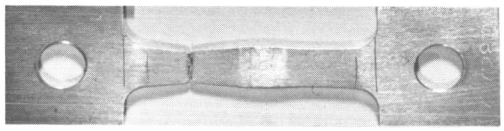
C3CU-4

Weld Failure

Uncontaminated
105 ppm Oxygen



12,168 60X



C3CI-2

Base Metal Fracture

580 ppm Oxygen

No Test
880 ppm Oxygen

FIGURE 40 - FS-85, Photographs of 2200°F Tensile Specimens

V. REFERENCES

1. G. G. Lessmann and D. R. Stoner, "Determination of the Weldability and Elevated Temperature Stability of Refractory Metal Alloys", First Quarterly Progress Report, WANL-PR-(P)-001.

2. G. G. Lessmann and D. R. Stoner, "Determination of the Weldability and Elevated Temperature Stability of Refractory Metal Alloys", Second Quarterly Progress Report; WANL-PR-(P)-002.

3. G. G. Lessmann and D. R. Stoner, "Determination of the Weldability and Elevated Temperature Stability of Refractory Metal Alloys", Fifth Quarterly Progress Report, WANL-PR-(P)-005, CR-54232.

4. G. G. Lessmann and D. R. Stoner, "Determination of the Weldability and Elevated Temperature Stability of Refractory Metal Alloys", Third Quarterly Progress Report, WANL-PR(P)-003, CR-54088.

5. G. G. Lessmann and D. R. Stoner, "Determination of the Weldability and Elevated Temperature Stability of Refractory Metal Alloys", Fourth Quarterly Progress Report, WANL-PR-(P)-004, CR-54166.

6. G. G. Lessmann, "The Comparative Weldability of Refractory Metal Alloys", The Welding Journal, to be published.

7. G. G. Lessmann and D. R. Stoner, "Determination of the Weldability and Elevated Temperature Stability of Refractory Metal Alloys", Eighth Quarterly Progress Report, WANL-PR-(P)-008, CR-54723.

8. G. G. Lessmann and D. R. Stoner, "Determination of the Weldability and Elevated Temperature Stability of Refractory Metal Alloys", Seventh Quarterly Progress Report, WANL-PR-(P)-007, CR-54434.

9. G. G. Lessmann and D. R. Stoner, "Determination of the Weldability and Elevated Temperature Stability of Refractory Metal Alloys", Ninth Quarterly Progress Report, WANL-PR-(P)-009, CR-54923.

10. R. T. Begley, et al, "Development of Niobium Base Alloys", Technical Report No. WADC-TR-57-344, Part 6, Feb. 1963.

11. R. L. Ammon and R. T. Begley, "Pilot Production and Evaluation of Tantalum Alloy Sheet", Summary Phase Report, WANL-PR-M-004, June 15, 1963.

12. R. W. Buckman and R. C. Goodspeed, Personal communication.

V. REFERENCES (Continued)

13. R. W. Buckman and R. C. Goodspeed, "Development of Dispersion Strengthened Tantalum Alloys", Ninth Quarterly Progress Report (NASA-CR-72020), Contract NAS 3-2542, Westinghouse Astronuclear Laboratory.